HELLENIC REPUBLIC
National and Kapodistrian University of Athens
EST. 1837

ΕΘΝΙΚΟ ΙΔΡΥΜΑ ΕΡΕΥΝΩΝ
National Hellenic Research Foundation

NATIONAL KAPODISTRIAN UNIVERSITY OF ATHENS

INTERDISCIPLINARY M.Sc. COURSE IN "NANOMEDICINE"

ACADEMIC YEAR 2018-2019

PREPARATION AND CHARACTERIZATION OF CHIMERIC/HYBRID LIPOSOMES WITH FUNCTIONAL COPOLYMERS

THEODOROS A. SENTOUKAS

SUPERVISOR: ASTERIOS PISPAS

COMMITEE MEMBERS: CONSTANTINOS DEMETZOS, ANASTASIA PIPPA

AUGUST 2019

AKNOWLEDGEMENTS

I would like to thank both Dr. Asterios Pispas and Dr. Constantinos Demetzos for passing their knowledge, for trusting me on this study and for allowing the usage of their equipment at the Institute of Theoretical and Physical Chemistry (National Hellenic Research Foundation) and at the Laboratory of Pharmaceutical Nanotechnology (National and Kapodestrian University of Athens) respectively. I would also like to thank PhD Candidate Maria Choundoulessi and Dr. Nikolaos Naziris for giving me the proper guidance on the preparation of liposomes.

Finally, I would like to thank my wife Stavroula, and my family, Angelos, Katerina, Nikolaos, Evangelos and Maria, for tolerating and supporting me, both mentally and financially.

TABLE OF CONTENTS

ABBREVIATIONS

AIBN 2,2'-Azobis isobutyronitrile

DLS Dynamic Light Scattering

DMPC 1,2-dimyristoyl-sn-glycero-3-phosphocholine

NMR Nuclear Magnetic Resonance

PDMAEMA Poly 2-dimethylamino ethyl methacrylate

PSMA Poly Stearyl Methacrylate

SEC Size Exclusion Chromatography

SLS Static Light Scattering

ABSTRACT

The purpose of this study is to prepare stimuli responsive hybrid/chimeric liposomes containing functional copolymers and conduct aqueous solution studies in order to determine their properties and potential as potential drug-delivery nanocarriers. Two random copolymers, composed of a hydrophilic, pH and thermo-responsive DMAEMA (dimethyl amino ethyl methacrylate) monomer and a hydrophobic SMA (stearyl methacrylate) monomer, were synthesized via free radical polymerization and molecularly characterized using SEC, FTIR, and ^{1}H-NMR. The synthesis was followed by aqueous solution studies utilizing dynamic and static light scattering in order to determine their stimuli responsive self-assembly properties. The preparation of chimeric-hybrid liposomes was mediated by thin film deposition and hydration, followed by aqueous solution studies via dynamic light scattering, ζ-potential and fluorescent spectroscopy. The drug-loading study is comprised of curcumin loading via a thin film deposition and hydration technique, while aqueous solution properties will be determined utilizing DLS, and UV-Vis spectroscopy.

INTRODUCTION

Nanotechnology is one of the most promising scientific concepts of the 20th century, as it unveils materials with novel and enhanced properties for applications in electronics, mechanics,[1] energy harvesting[2] and medicine.[3, 4, 5] It comprises an integration of multiple scientific fields, such as physics, chemistry, engineering and biology and refers to the imaging, measuring, modeling and manipulating matter in molecular and nanometer level scale, resulting in materials with one or more dimensions in the nanoscale. The latter refers to size between 1-100 nm, where properties differ significantly from those at larger scale, presenting unique phenomena that enable novel applications. Although the sudden rise of its popularity over the last decade, nanotechnology was known to humanity for thousands of years, with Lycurgus Cup (a mixture of gold/silver nanoparticles embedded into a glass matrix), and Damascus steel (with cementite nanowires and carbon nanotubes), to be the most characteristic examples.

Figure 1: The Cup of Lycurgus, illustrating the myth of King Lycurgus, who is kidnapped by the Greek nymph Ambrosia and brought to the underworld. Reflected light makes the cup appear green, while transmission light turns the cup red.[6]

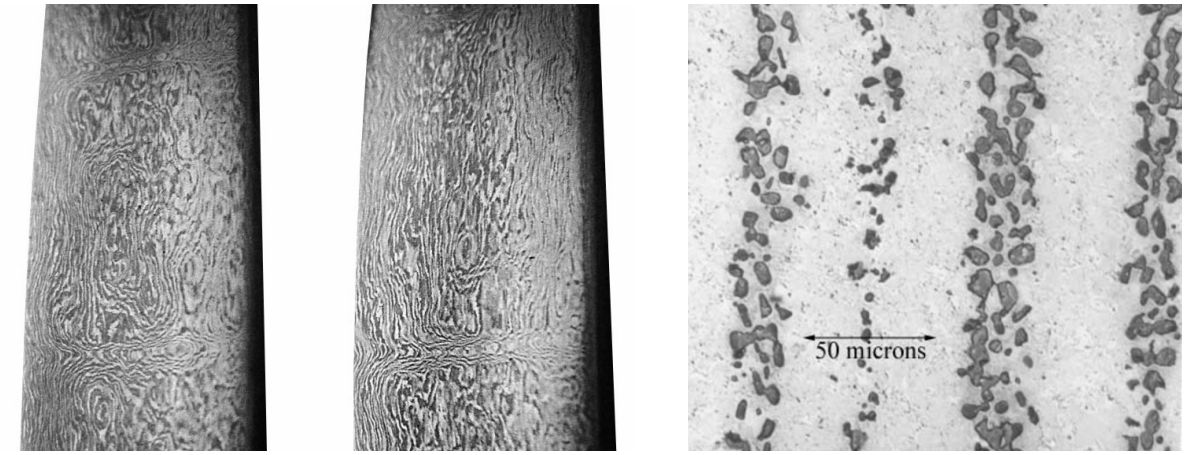

Figure 2: Damascus steel blade patterns (left) and the carbide nanoparticles forming aligned rows inside the blade (right).[7]

Richard Feynman was the first to envision the development of nanoscale machines that "*arrange the atoms the way we want and mediate chemical synthesis by mechanical manipulation*" and explained his concepts and ideas in his famous talk "*There is plenty room at the bottom*" in 1959 at the California Institute of Technology. A few years later, in 1974, Norio Taniguchi coined the term of nanotechnology by saying that "*Nanotechnology mainly consists of the processing, of separation, consolidation, and deformation of materials by one atom or by one molecule*". Finally, Kim Eric Drexler, inspired by Feynman's concepts, described in his book in 1986 what later became known as molecular nanotechnology. He proposed the idea of a nanoscale assembler, which would be able to replicate itself and build systems of random complexity with atomic control.[8-10]

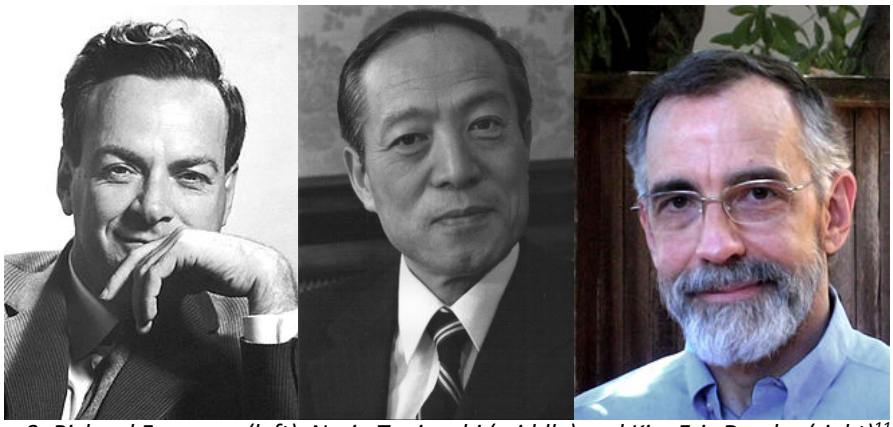

Figure 3: Richard Feynman (left), Norio Taniguchi (middle) and Kim Eric Drexler (right)[11-13]

Organic, inorganic, metallic, carbon based, or even hybrid/chimeric, a plethora of different kinds of nanomaterials have been developed until now, with various shapes and morphologies (e.g. nanowires, nanotubes, nanospheres, nanorods, vesicles, nanoworms) targeting on

multiple applications. Nanomaterials can be classified according to their dimensionality as 0-D (quantum dots) if all external dimensions are on the nanoscale, 1-D if only one external dimension on the nanoscale, 2-D if two external dimensions are on the nanoscale, and 3-D if none of the external dimensions are on the nanoscale. The key reason behind the different properties of nanosized materials against bulk materials lies to large surface area/volume ratio and as a result, gravitational forces become negligible at the nanoscale, while instead, quantum effects and electromagnetic forces become dominant. [8-10]

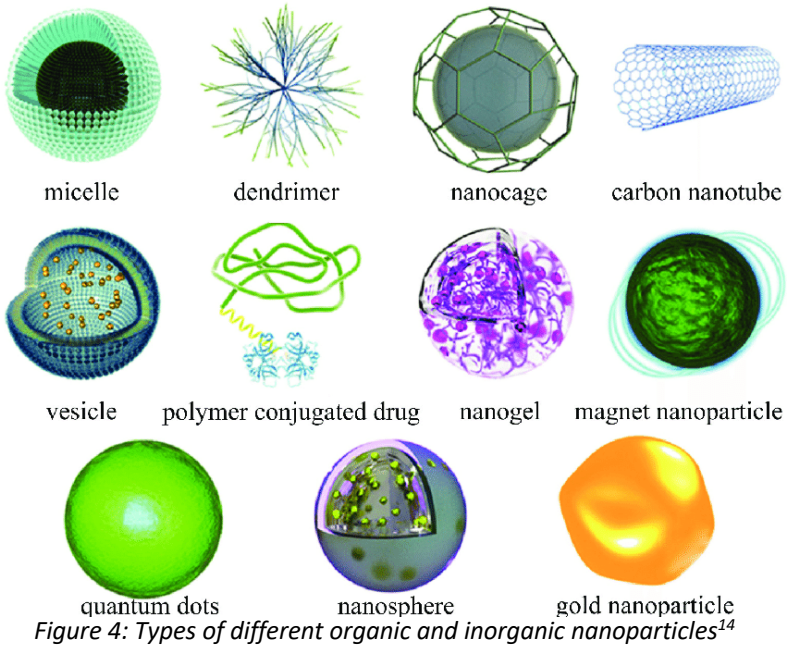

Figure 4: Types of different organic and inorganic nanoparticles[14]

Nanomedicine is the medical implementation of nanotechnology and refers to the design, development and use of nanosized materials, nanoparticles, biological devices, biosensors, systems or even biological machines for diagnosis, prevention and treatment of disease and to gain increased understanding of the complex underlying pathophysiology of disease. The ultimate goal is to improve quality of life. Current applications of nanomedicine are drug/gene/protein delivery, contrast agents for ultrasound, MRI and CT Scan, lab-on-a-chip, blood purification, tissue engineering, orthopedic surgery, vaccines even the more edgy and futuristic nanomedical machines.[5, 15, 16]

Drug delivery is the process of administration, transportation, controlled and/or sustained release of an active pharmaceutical ingredient (API), loaded into a nanocarrier in order to either target actively or passively the infected tissue, maximize the dosage and bioavailability and minimize the side effects. Polymers, liposomes, metallic and inorganic nanoparticles, are

amongst the best candidates and their combinations form an army of advanced drug delivery nanosystems. These ADDnSs have to be designed precisely in order to exploit several pathological factors, such as the enhanced permeability and retention effect (EPR) of the pathogenic epithelial tissues, acidic pH and increased temperature surrounding tumor cells. Also, protein and/or genes can be bound on/encapsulated in nanoparticles, creating a biological corona, avoiding immune response and transferring proteins/genes to certain cells for repairing genetic diseases.[5, 17-20]

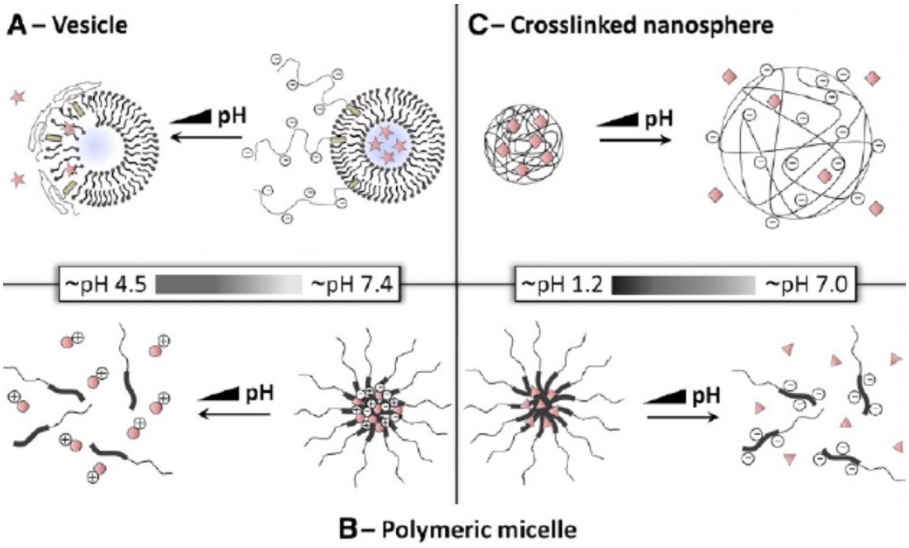

Figure 5: Typical example of structure destabilization/collapsing of pH-responsive ADDnSs after changing the environmental pH values, resulting in the release of the entrapped drug.[21]

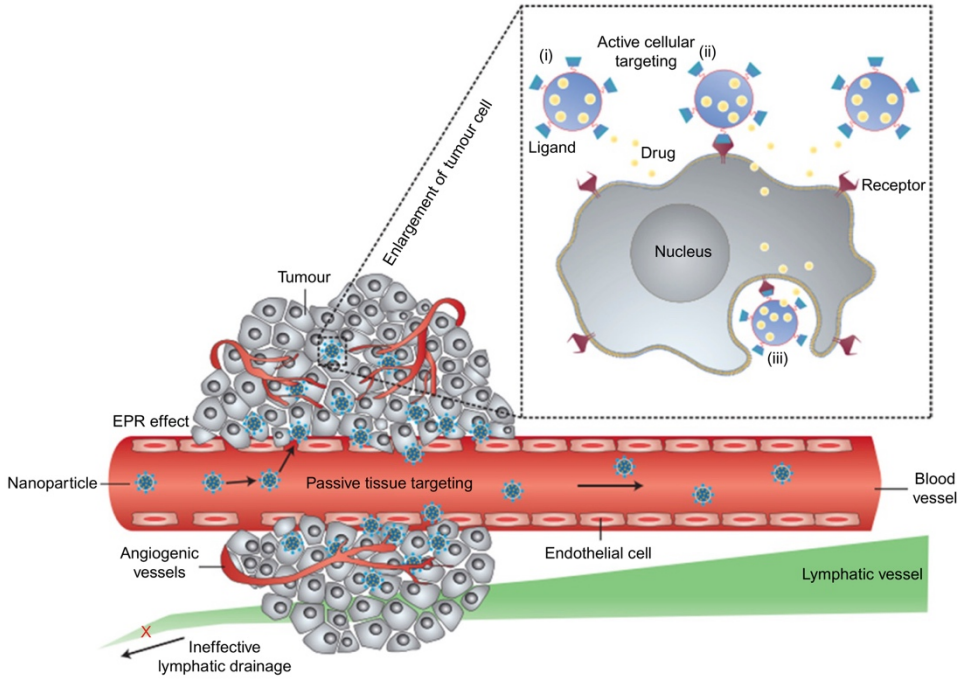

Figure 6: Schematic draw of the EPR effect in a tumor site.[20]

Ultrasound, Magnetic Resonance Imaging (MRI) and CT scan are medical techniques used for imaging internal organs and identifying primary and/or metastatic tumors, blood pooling, ischemia, angiogenesis, atherosclerosis, inflammation and drug distribution. In order to enhance the resulting image and increase the contrast of structures or fluids, chemical substances must be utilized, called contrast agents. Each imaging technique uses different contrast agents and the current standards are iodine and barium (X-rays), gadolinium and fluorinated dyes (MRI), micro and nanobubbles (ultrasound).[22-24]

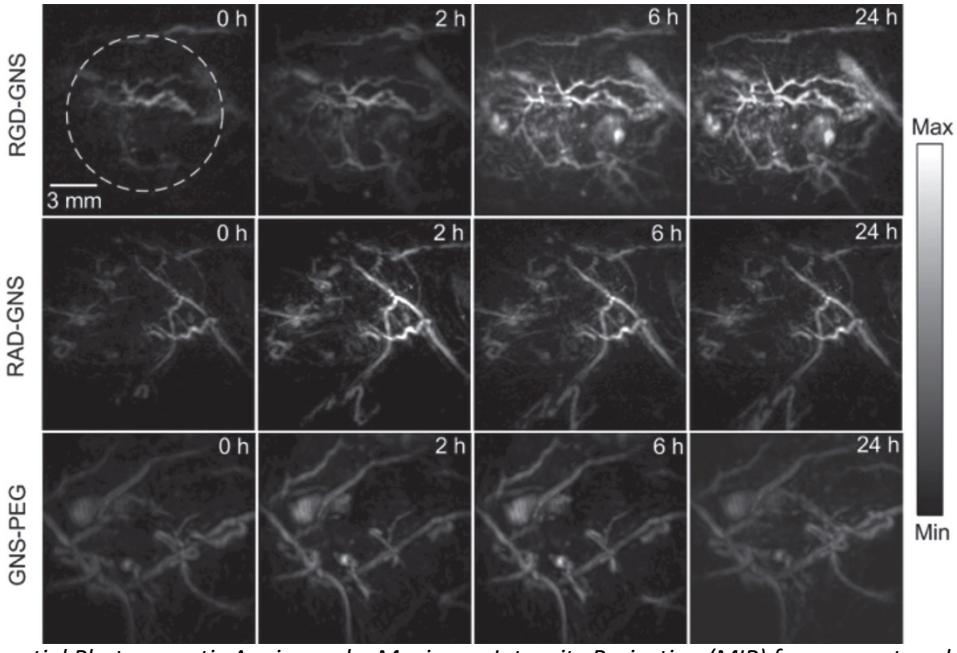

Figure 7: *Sequential Photoacoustic Angiography Maximum Intensity Projection (MIP) frames captured before, 2, 6, and 24 h post-injection of the RGD-GNS (upper panel), RAD-GNS (middle panel) and GNS-PEG (lower panel) through tail vein.*[24]

Lab-on-a-chip technology has been a very useful project for detection of a variety of protein, biomarkers and nucleotides for cancer and diabetes diagnosis, amongst others. Gold and metallic nanoparticles tagged with short segments of DNA,[25] quantum-dots-embedded polymeric nanobeads[26] and nanowires[27] are a few to name. Certain devices equipped with nanowire sensors of various markers, each one specialized for the detection of different pathological cause (glucose levels[28], cancer[29], etc.).

Regenerative medicine and tissue engineering refer to the reproduction or reshaping damaged tissue utilizing a combination of biocompatible and biodegradable polymeric-based scaffolds, reinforced with graphene, carbon nanotubes, molybdenum disulfide or tungsten disulfide nanoparticles, with embedded growth factors and stem cells. The scaffold provides

both mechanical support and nourishment for stem and newborn cells, while growth factors stimulate cell mitosis and reproduction.[30, 31]

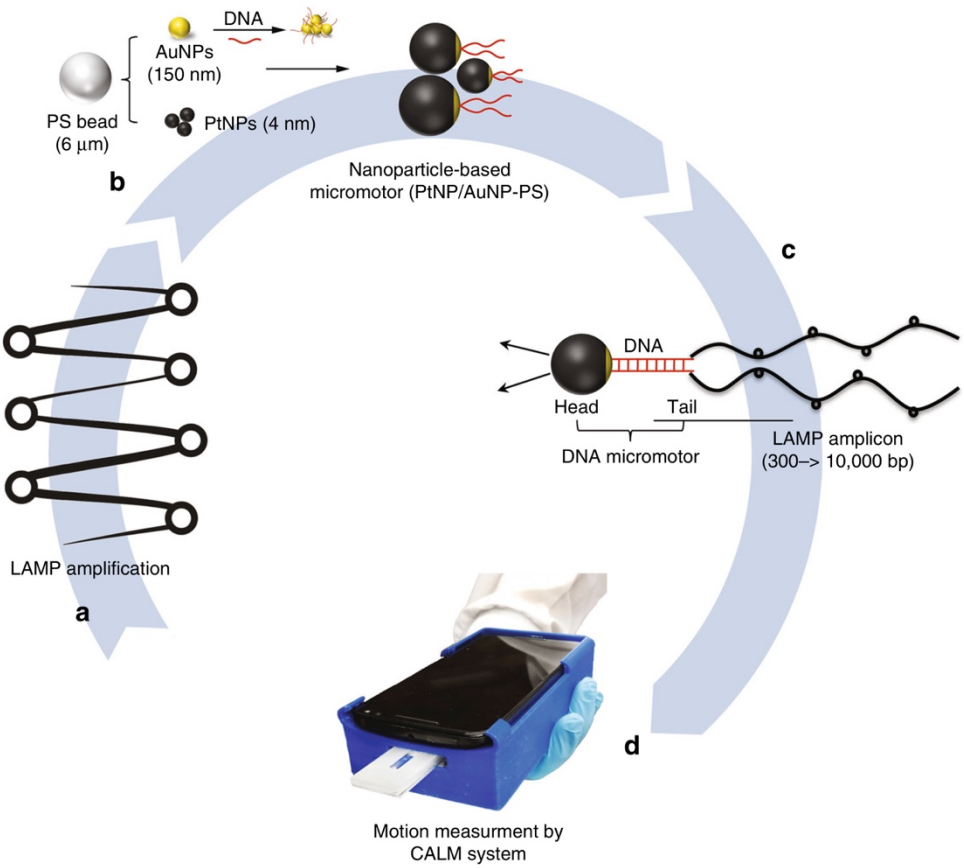

Figure 8: Schematic presentation of HIV-1 detection using the cellphone system. ***a)*** *The HIV-1 nucleic acid is amplified utilizing a loop-mediated isothermal amplification (LAMP).* ***b)*** *A polystyrene (PS) beads covered with a hybrid surface layer of platinum (Pt) and gold (Au) nanoparticles system is prepared that presents catalytic motion in a hydrogen peroxide solution,* ***c)*** *The amplified nucleic acid is complexed with the previous system,* ***d)*** *A cellphone is able to detect and measure the motion of the catalytic head of motors with large DNA tails.*[25]

Orthopedic surgery is a medical field that utilizes biomaterials in order to deal with bone and/or joint injuries or surgery rehabilitation. Panels, osteosynthesis screws and artificial joints are a few implant solutions for bone fractures and joint degeneration. Before designing such implants, one must take into consideration the osseointegration effect (the interaction between the implant and the native bone), microbial infestations, bone tumors and fractured surfaces filling. Certain nanotextured implant surfaces have augmented the function and growth of osteoblasts to increase implant osseointegration, while nanocrystallic hydroxyapatite can fill the empty space of fractured areas. Selenium nanoparticles can be utilized to the implant surface to suppress bone tumors, while silver nanoparticles with IL-12 nanocoatings provide anti-microbial action against infestations.[31, 32, 33]

Vaccines are biological agents that improve the immune system against a particular disease and still remain the most cost-effective way to prevent infections. While traditional vaccines are comprised of antigens based on surface proteins, virus parts, deactivated pathogens, or bacterial toxins, new age nanovaccines carry extra immunostimulant agents, called adjuvants, bound to the specific antigen in order to induce maximal immune response. Liposomes, virosomes and polymeric nanoparticles are some examples of adjuvant systems, enhancing antigen delivery, uptake by appropriate cells and induction of stimulatory cytokines and chemokines.[34-37]

Nanomaterials have gained a great deal of publicity through the last decade due to their exceptional properties and novel applications, but all that glitters are not gold. Production costs remain high and sometimes there are differences from batch to batch, since they are highly chaotic systems. Their large active surface area can be a potential health hazard even at their early stage of production and must be handled very cautiously. Also, since they are novel materials, toxicity studies are yet to be carried through and long-term use consequences for humans are not known. Last but not least, the environmental impact must be taken into consideration, while piling up into the soil and water contamination can become calamitous for the natural reserves and even further a health hazard for humans.[38-40]

Clearly, nanomedicine is a rather new and promising concept, with thousands of studies, patents and commercial products. The whole field is strongly connected with the concept of personalized medicine, with a growing number of nanotechnology and nanomedicine products have been reported the past years. More specifically, by the end of 2015, more than 40 marketed products and over 300 in development have been reported. The current US market value is estimated at 12 billion dollars, while the generated income is calculated at 1000 billion euros by the end of 2015 and it is expected to double-increase by the end of 2020.[5, 41, 42]

THEORY

Polymers

Polymer nanoparticles have conquered the world rapidly over the last decades, filling the needs of a wide spectrum of applications in electronics, energy harvest and storage, engineering and medicine. Having a wealth of synthesis techniques, one can literally design and manufacture the exact architecture needed for the specific application. Polymer nanoparticles have been extensively used in nanomedicine as advanced drug/protein/gene delivery nanosystems, as scaffolds in tissue engineering, as anti-microbial coatings, as vaccine adjuvants, as bio-interfaces in regenerative medicine, as functionalized nanoparticles for site-specific imaging and therapeutics, and as stabilizers and immune-avoidance in PEG-ylation.

The word Polymer derives from the Greek "*πολύ*" (many) and "*μέρη*" (parts). Each part is called monomer, or repeating unit. Polymers are "large chain-like molecules (macromolecules) built up by the repetition of small chemical units" and the number of repeating units in each chain is called "*degree of polymerization*" (DP), specifying the length of the polymer molecule. Polymerization is the process of polymer synthesis and refers to the progressive reactions of repeating units (monomers), leading to a consecutive series of reactions mediated as the repeating units are coupled together forming the polymer chain.

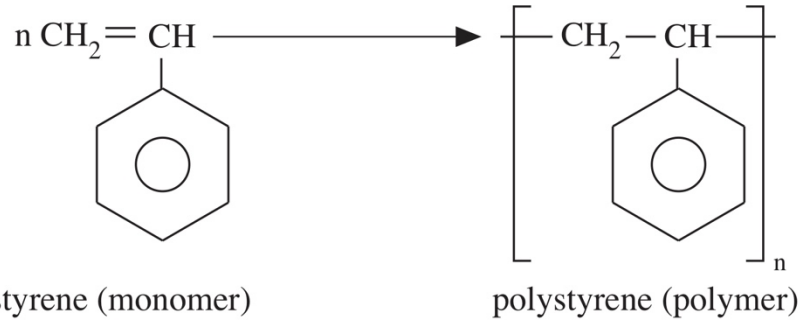

Figure 9: Schematic representation of a styrene monomer (left) and its equivalent formed polymer (right).[43]

Polymer classification can be carried out based on their:

- Origin (natural or synthetic),
- Structure (linear, branched, cross-linked),
- Polymerization mechanism (step-growth, chain-growth),
- Composition (homopolymer, copolymer),

- Preparative techniques (bulk, solution, suspension, emulsion polymerization),
- Mechanical properties (fibers, plastics, elastomers)
- Crystallinity (amorphous, crystalline),
- Thermal behavior (thermoplastics, thermosets).

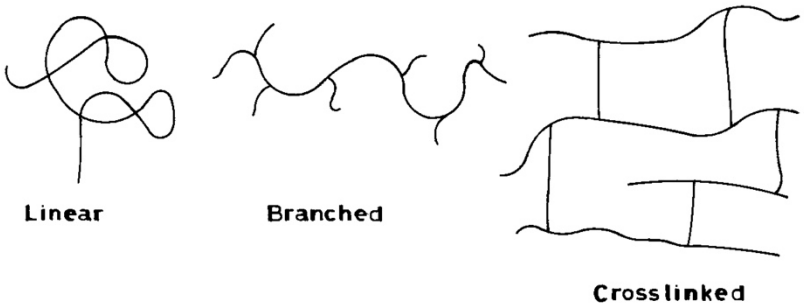

Figure 10: Schematic illustration of linear (left), branched (middle) and cross-linked polymers (right).[43]

Natural occurring polymers are synthesized by living organisms and include proteins, enzymes, cellulose, while synthetic polymers are man-made polymers, such as polyurethane, polyesters, polyethylene, nylon etc. Regarding their structure, polymers can be grouped into linear, branched or cross-linked, based on their interlinking capacity, meaning the number of sites available for polymerization. Thus, a monomer can be mono-functional, difunctional, or even multifunctional.

The polymerization mechanism responsible for their formation further categorizes polymers into step-growth and chain-growth prepared polymers. Step-growth polymers are slowly formed by the stepwise reaction between functional groups of monomers, containing heteroatoms, such as nitrogen or oxygen. Chain-growth polymers are formed by the linkage of unsaturated monomers, containing double or triple carbon-carbon bonds. An initiator molecule, which could produce a free-radical, an anion, or a cation, is required to break the unsaturated bonds and create an available site for polymerization and thus, a carbon-only polymeric backbone is formed. Four main types of chain-growth polymerization are reported, free-radical, anionic, cationic and ring-opening polymerization.

Polymeric nanoparticles can be either homopolymers if composed of only one kind of monomers, or copolymers if composed of two different kinds of monomers. More monomer kinds have reported on certain studies, and so polymeric nanoparticles are classified as terpolymers (three kinds), quadropolymers (four kinds) or penta-polymers (five kinds). Further

classification based on the composition can be given regarding the type of order a monomer has in the backbone. Four types of copolymers have been named so far:

- Random copolymers, where the different monomers are randomly arranged on the polymer chain,
- Alternating copolymers, where the different monomers are arranged alternatively along the polymeric chain,
- Block copolymers, where the polymeric backbone consists of large sequences (blocks) of each monomer, one after another.
- Graft copolymers, where sequences of one monomer are "grafted" onto the chain (backbone) of another monomer.[43-46]

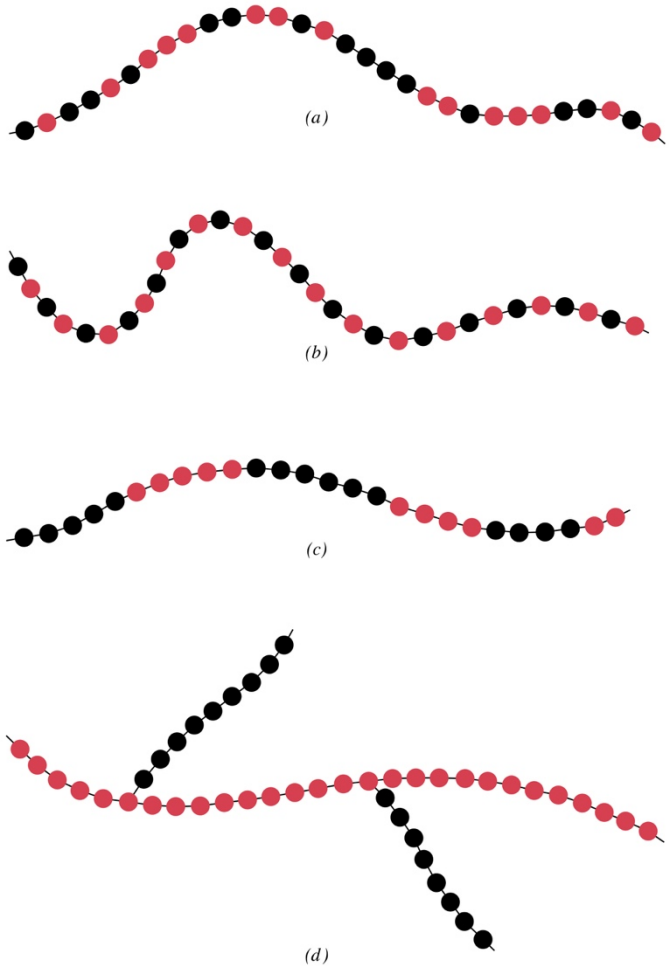

Figure 11: Classification of copolymers in a) random, b) alternating, c) block and d) grafted.[47]

Polymerization techniques can be further classified into four categories:

- Bulk polymerization, in which only the monomer, along with a catalyst is fed into the reactor and extracted as a solid mass,
- Solution polymerization, in which both the monomer, the catalyst and the formed polymer are soluble in the same solvent,
- Suspension polymerization, in which the monomer and the catalyst are dispersed into an aqueous medium and the resulting polymer forms a solid dispersion and
- Emulsion polymerization, in which the monomer and the resulting polymer constitute the disperse phase, while the catalyst is solubilized into the aqueous medium. [43-46]

Stimuli responsive polymers comprise a special category of smart polymeric nanoparticles that can change their physicochemical properties when exposed to certain physical or chemical environmental conditions, mimicking the behavior of living cells. These environmental conditions can be internal (endogenous), or regulated by an external factor (exogenous). Endogenous conditions refer to native temperature, pH, redox environment, hypoxia, ATP, glucose and enzymes concentration, while exogenous stimuli are related to temperature change, light, ultrasound, electrical and magnetic fields. Due to their special abilities, stimuli responsive polymers have been used in nanomedicine, especially in targeted and controlled-release drug delivery applications.[48-50]

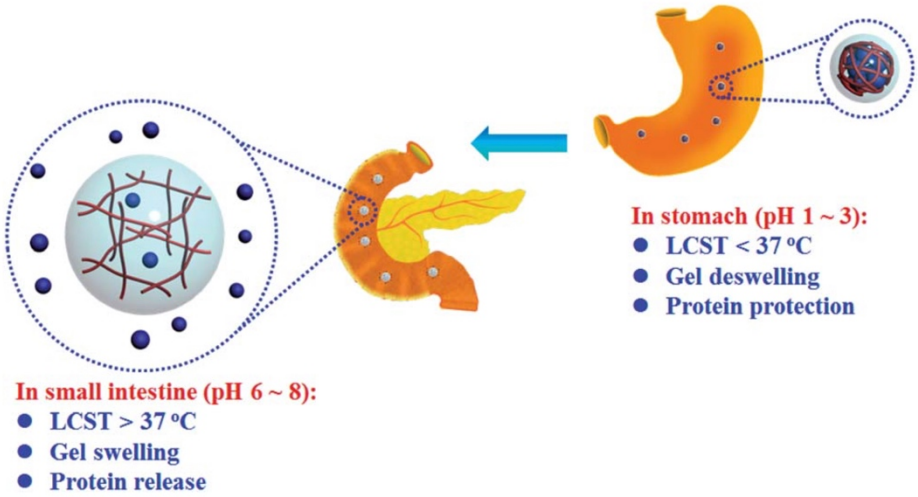

Figure 12: Representation of the drug-release behavior of a pH and thermo-responsive hydrogel in the stomach and small intestine sections.[51]

Poly (Dimethyl Amino Ethyl Methacrylate) and Poly(Stearyl Methacrylate)

Poly (Dimethyl Amino Ethyl Methacrylate) (PDMAEMA) is a pH and thermo-responsive polymer with pK_a=7.3 at 25°C and a Lower Critical Solution Temperature (LCST) around 45°C, depending on molecular weight and pH of the aqueous solution. The latter depicts the hydrophilicity of the PDMAEMA at temperatures under the LCST, while a temperature increase over the LCST leads to the breakage of hydrogen bonds between the polymer and water molecules, resulting into a more hydrophobic character. At pH 3, PDMAEMA is fully protonated, fully soluble in water and thus loses its thermo-responsive behavior. At pH 7, PDMAEMA is partially protonated and exhibits a thermal transition in the form of LCST, which depends mostly on its molecular weight.[52, 53] On the other hand, Poly (Stearyl Methacrylate or Octadecyl Methacrylate) (PSMA) comes with a long hydrocarbon crystallizable side chain, making it a highly hydrophobic polymer.[54]

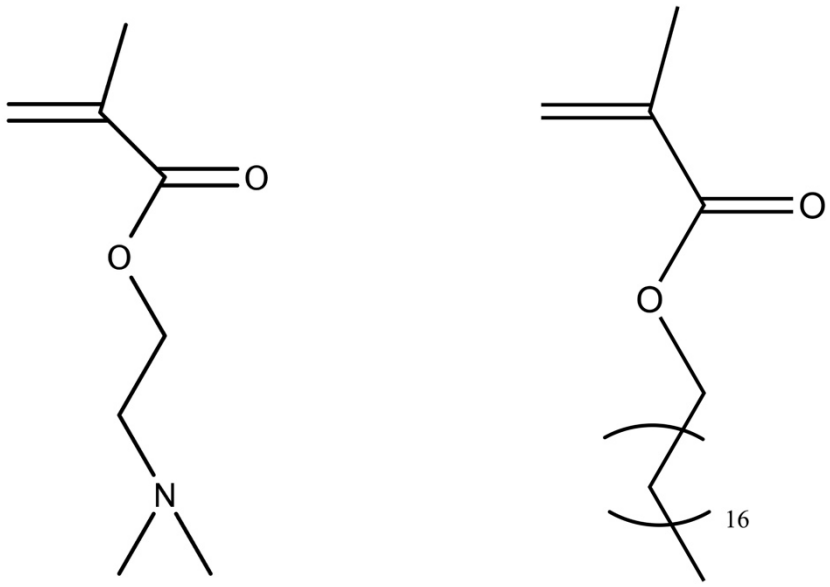

Figure 13: Schematic illustration of PDMAEMA (left)[53] and PSMA (right)[54].

Free-Radical Polymerization

Free-radical polymerization is a chain-growth polymer synthesis technique, utilizing an initiator molecule that produces free-radicals R* (e.g. molecules with an unpaired valence electron) and transfers them to a carbon-carbon double-bond containing monomer, producing a new type of free-radical, which in turn is transferred to new monomers added to the initial free-radical. This sequential addition of new monomers to the initial free-radical leads to the final polymeric chain synthesis.

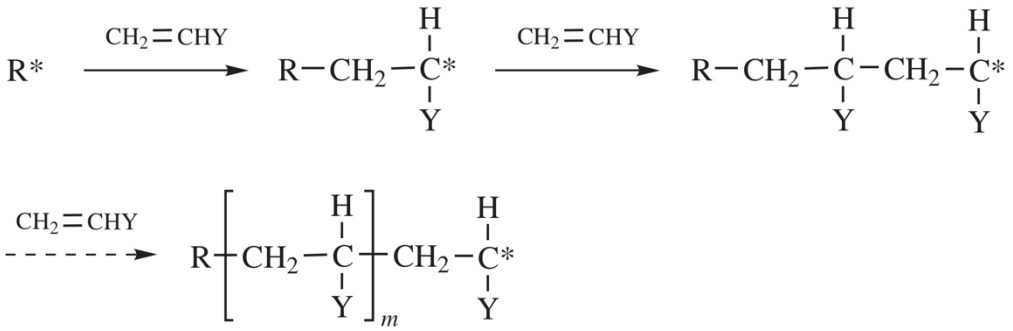

Figure 14: Typical example of a free-radical polymerization procedure. The R species transfers to the monomer by breaking the carbon-carbon double-bond, forming an active site for further monomer addition.*[43]

A macromolecular polymeric chain is synthesized via free-radicals in a three-step procedure:

- Initiation
- Propagation
- Termination

The initiation phase is comprised of two steps, the production of free-radicals and the formation of an active monomer site responsible for the polymerization initiation,

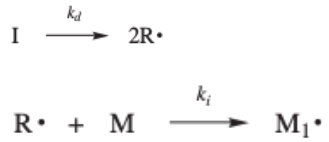

where M represents the monomer, M_1* represents the active site monomer and k_d and k_i the constants of dissociation and initiation respectively. The free-radical R* emerges from an initiator I via chemical, thermal or photochemical external stimuli.

The propagation phase consists of the length increase of the M_1* by successful addition of hundreds or maybe thousands of monomers, as depicted below:

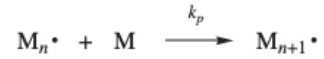

with k_p representing the propagation constant, with values ranging from 10^2-10^4 L mol^{-1} s^{-1} for most monomers.

The termination stage occurs when the active site is eliminated by intermolecular reactions between two free-radicals. This can happen either by a coupling reaction or disproportionation as depicted below:

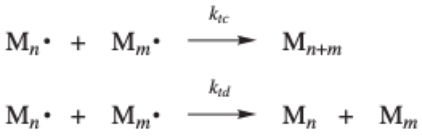

where $k_t = ak_{tc}+(1-a)k_{td}$ and a and (1-a) the termination fractures by coupling and disproportionation respectively.[43-46]

Liposomes

Liposomes have been extensively used over the last 30 years in various applications, especially in targeted drug delivery for cancer treatment and cosmetics due to their exceptional biocompatibility and biodegradability, since they are cell's membrane copycuts. [55] The word "liposomes" derives from the Greek words "λίπος" (fat) and "σώμα" (body), since they are mostly comprised of phospholipids. Alec D. Bangham and R. W. Horne were the first ones to discover their bilayer formation accidentally in 1961, while they were testing a new electron microscope by adding negative-stain on dry phospholipids.[56, 57] These lipid structures were originally named "multilamellar smectic mesophases" or even "Banghasomes", but it was Gerard Weissman, an emeritus professor at the New York University School of Medicine, who later on proposed the now-established term "liposomes".[58, 59]

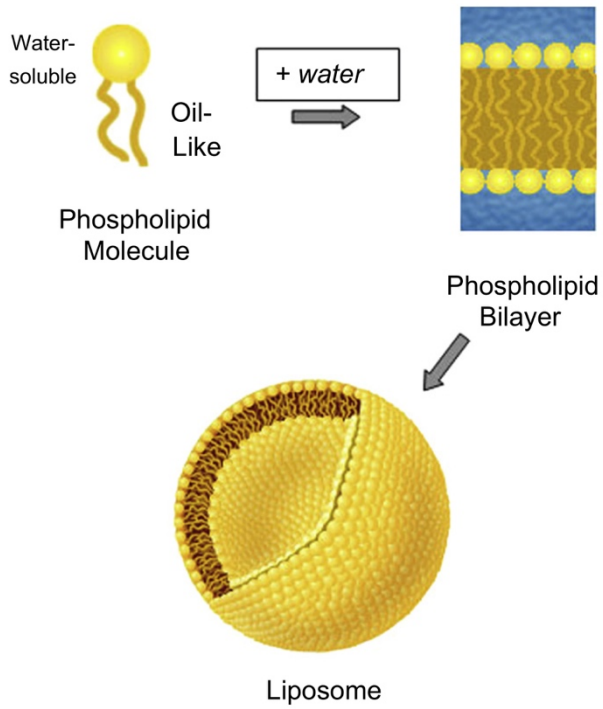

Figure 15: Schematic illustration of phospholipids (upper left), liposomes (down) and phospholipid bilayer cross-section (upper right).[55]

Phospholipids are composed of a hydrophilic head, consisted of a polar phosphate group and two hydrophobic fatty acid tails joined together by a glycerol molecule. When introduced into aqueous media at a low concentration they form lipid bilayers with the hydrophilic heads forming hydrogen bonds with water, while the hydrophobic tails turn to each other to avoid interactions with the aqueous media. This self-assembly is a spontaneous procedure, leading

the dispersed and disordered phospholipids into forming a certain pattern, as a result of hydrophobic interactions between the phospholipids and the aqueous media, in order to minimize system's free-energy.

Increasing phospholipids' concentration over a certain threshold (30 mg/mL) inside the aqueous medium leads to the formation of hollow, pseudo-spherical vesicles, comprising of at least one lipid bilayer. Systems that depend on concentration for their final formation are called lyotropic. Another interesting fact about the aforementioned structures is the fluidity of their bilayer, since phospholipids are constantly moving across the membrane, mimicking the lipid bilayer found on a human cell. This fluidity renders such structures as liquid crystals, since they are metastable forms of matter, meaning they are nor solid, nor liquid, but something in between.

So, what exactly are liposomes and how can they be prepared? Liposomes, by definition, are lyotropic liquid crystal, colloidal dispersion systems, self-assembled in one or more vesicle-like pseudo-spherical dynamic (fluid) lipid bilayers. They can be classified as multilamellar vesicles (MLV), small unilamellar vesicles (SUV) and large unilamellar vesicles (LUV). Each bilayer mainly consists of phospholipids and cholesterol, with polar heads oriented towards the aqueous medium, while lipophilic tails and cholesterol face the other way in order to avoid hydrophilic interactions.[17, 55, 60, 61] Small molecules or polymers can be docked on the surface of the bilayer amphiphilic, and hydrophobic molecules/drugs can be entrapped within the lipophilic tails, manipulating liposomes' functionality and simulating the cell's membrane. [17, 62-64]

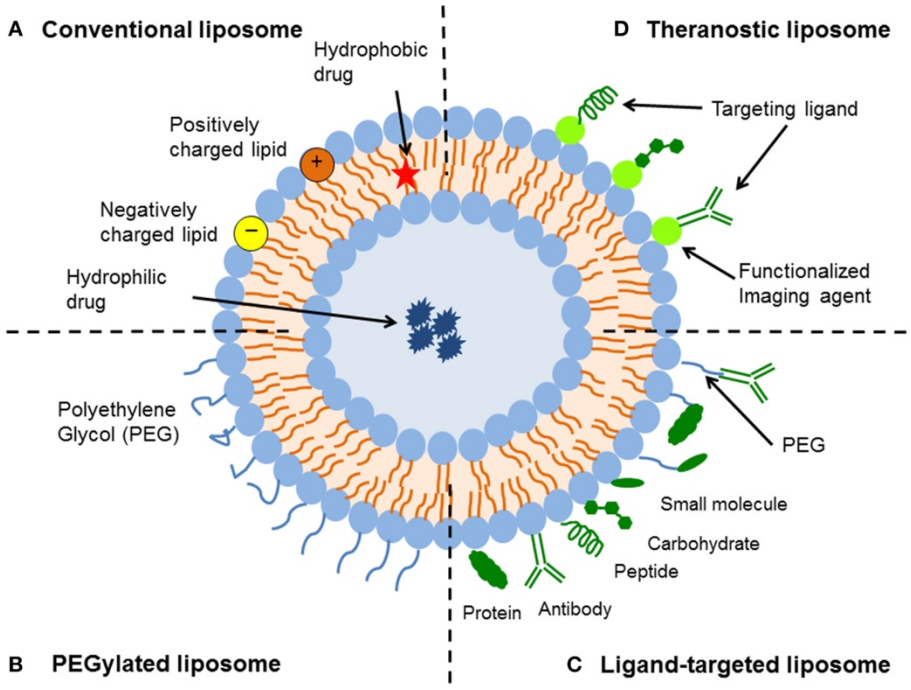

Figure 16: Schematic illustration of a functionalized liposome for different therapeutic purposes. A) Conventional liposome, with neutral or ionic phospholipids, a hydrophobic drug inside the bilayer and a hydrophilic drug inside the core. B) PEG-functionalized liposome in order to provide "stealth" properties and prevent an immune response. C) Ligand-functionalized liposome for active targeting and D) Theranostic liposome that is functionalized with imaging agents.[65]

While liposomes have gained a great deal of publicity over the last 50 years, due to their remarkable abilities, the progress made for their commercialization as drug delivery systems is nowhere near the expected. The liposomes clearance by the Reticuloendothelial System (RES), the interactions with opsonins, the Accelerated Blood Clearance Phenomenon (ABC), along with the Complement Activation-Related Pseudoallergy (CARPA) and certain instability issues pose great downsides for these particular systems. The PEGylation procedure provides "stealth" ability to the liposomes, inhibiting interactions with opsonins, allowing them to stay for more time in the blood circulation and thus avoid clearance by the RES. Even so, constant dosing with PEGylated liposomes leads eventually to the activation of immune system and the subsequent removal of the liposomes from blood circulation, the ABC phenomenon. Also, many liposomal systems, both experimentally and commercially available, activate an immune and inflammatory response, a phenomenon known as CARPA. Several approaches have been made in order to successfully minimize such immune responses, but more challenges are emerging, such as:

- Scalability,
- Reproducibility,
- Complexity of addition of ligands and surface modification,
- Denaturation over time,
- Long-term Stability,
- Complexity of the clinical trials.[65, 66]

Stimuli Responsive Chimeric/Hybrid Liposomes

Stimuli responsive chimeric/hybrid liposomes are a special category of hybrid systems that are comprised of liposomes with docked stimuli responsive amphiphilic polymeric chains. The hydrophobic part of the polymeric chain will be docked inside the lipophilic tails of the lipid bilayer, while the hydrophilic part of the polymeric chain will extend beyond the polar phospholipid heads. The main idea behind this concept is to provide the liposomes with extra stability, "stealth" properties, and functionality, such as pH- and thermo- responsiveness, for active targeting and controlled drug release.[19, 67-72]

Naziris et al. have shown that pH and thermo-responsive (co)polymers provide better and prolonged stability to the conventional liposomes, when mixed in certain molar ratios, while exhibiting interesting properties as drug delivery systems for active targeting in tumor sites that present an increased-temperature acidic environment.[67, 68, 70] Sang-Min Lee et al. prepared a chimeric liposomal system called polymer-cage nanobin (PCN) comprised of a cholesterol-terminated poly(acrylic acid), incorporated into liposomes and cross-linked with poly[(acrylic acid)-co-(acrylamide)], forming a cage around the liposome. They reported prolonged circulation time, through improved RES avoidance and an improved ability to complexate with biological macromolecules, such as genes or proteins. They also proposed the use of such PCN systems in personalized medicine.[72] Yamazaki et al. successfully prepared a dual-stimuli chimeric liposomal system, comprised of pH and thermo-responsive polymers for active targeting transdermal drug delivery. Studies have shown the successful release of the therapeutic agent from the liposomal bilayer when they reached the pathological tissue with certain pH and temperature environment.[69]

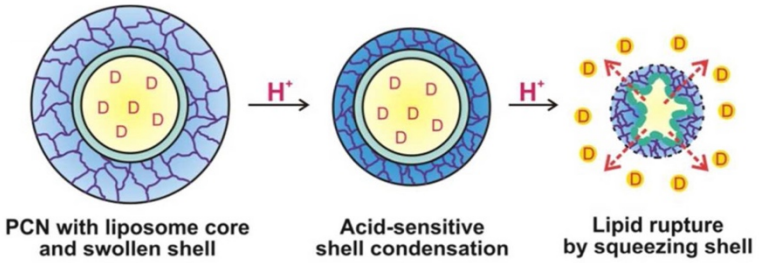

Figure 17: Schematic illustration of the release mechanism of a PCN liposomal system.[72]

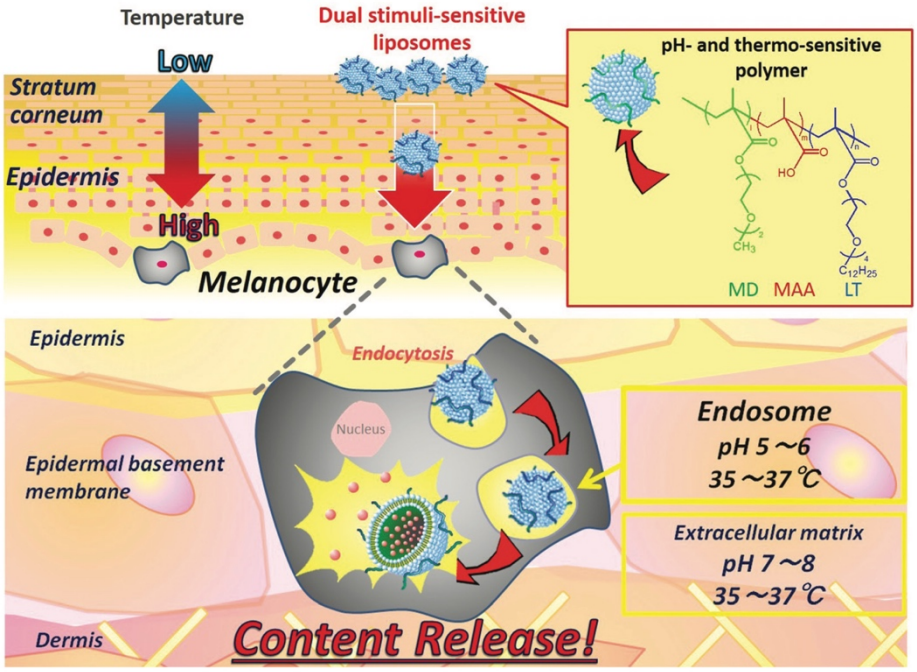

Figure 18: Dual stimuli with pH and thermo-responsive behavior chimeric/hybrid liposomes utilized as transdermal drug delivery system.[69]

CHARACTERIZATION TECHNIQUES

ATR-FTIR Spectroscopy

Attenuated Total Reflectance Fourier-Transform Infrared (ATR-FTIR) spectroscopy is the most known vibrational characterization technique that studies interactions between infrared light and matter, extracting information about the chemical composition of a sample. Its biggest advantages are:

- Fast, easy, inexpensive technique,
- Can analyze samples in all states of matter, even with a small amount of sample,
- Every detail regarding peak position, width, intensity and shape can provide extremely critical information about the sample structure and interactions.

The biggest disadvantages of this technique are:

- Some substances do not absorb infrared light,
- Complex composition samples are hard to identify/study,
- Aqueous solution samples are almost impossible to identify due to the fact that water is a strong infrared light absorber.

It is well known that light can behave both as a wave and as a particle. As a wave, it is comprised of an electric and a magnetic vector, perpendicular to each other, while as a particle, the so-called photon, an entity consisted of energy. The ATR-FTIR technique is based on the fact that infrared light can interfere with chemical bond vibrations, when absorbed by a sample. These vibrations, called normal modes, lead to stretching, contracting and bending of the chemical bonds and can be depicted in an infrared spectrogram. For a molecule to absorb infrared light two conditions must be fulfilled.

For the first condition, the interaction of the electric vector of light with a particular chemical bond should be able to create an induced dipole, due to the difference in electronegativity of atoms. The molecule absorbs infrared light and starts vibrating only when the ratio of the dipole moment to atoms distance within the molecule is non-zero, as shown in the following equation and Fig. 19:

$$D\mu/dx \neq 0 \quad (1)$$

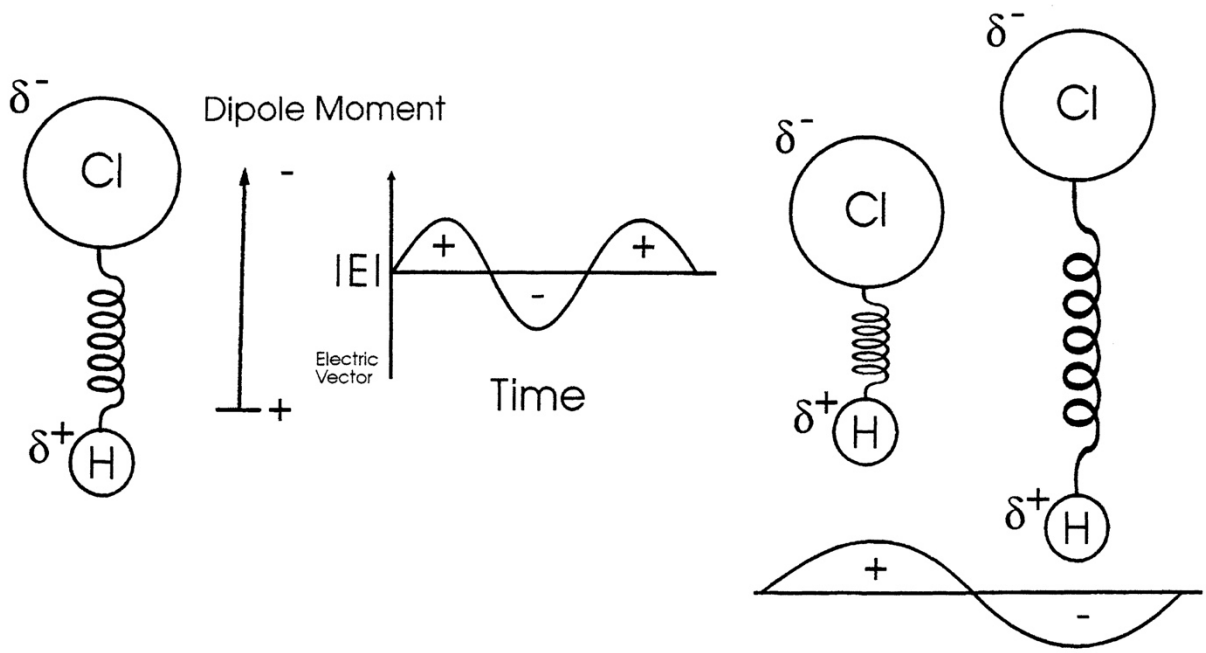

Figure 19: Interaction of the electric vector of a light beam with an HCl molecule, creating an induced dipole moment and forcing the molecule to vibrate.[73]

The second condition refers to the fact that the energy of the photon of the light beam should be equal with the vibrational energy level difference inside the molecule (Fig. 20) and fulfill the following equation

$$\Delta E_{vib} = hcW \quad (2)$$

where E_{vib} is the molecule's vibrational energy, h is the Planck's constant, c is the speed of light and W is the wavelength.[73, 74]

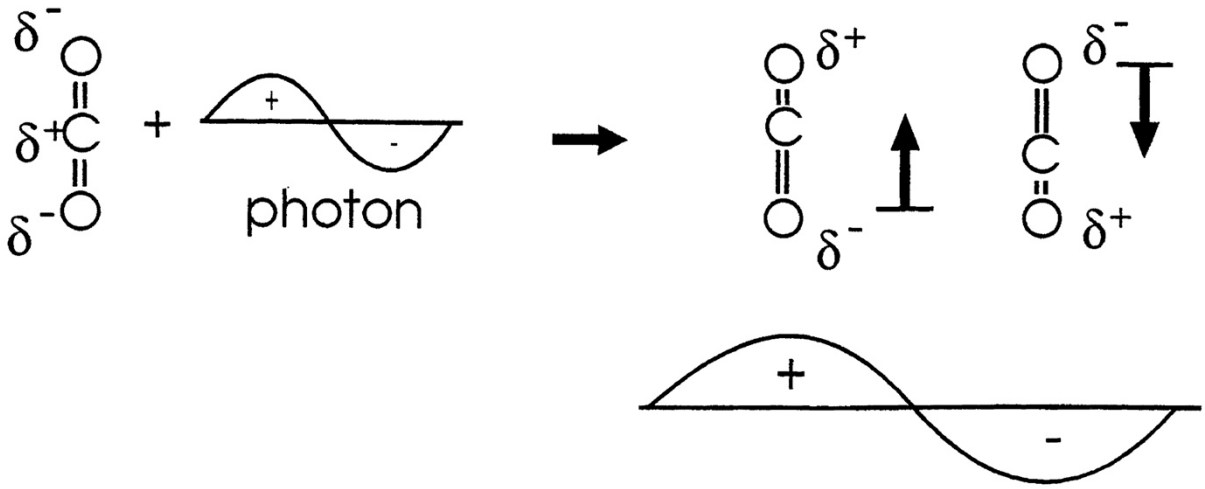

Figure 20: Interaction of the electric vector of a light beam with an CO_2 molecule, creating an induced dipole moment and forcing the molecule to vibrate.[73]

Nuclear Magnetic Resonance (NMR)

Nuclear Magnetic Resonance (NMR) is a spectroscopy characterization technique that provides information about chemical structure, composition, stereotactic and geometric isometry. It is based on the fact that each nucleus resonates in certain frequency due to the presence of surrounding electrons, which create local magnetic fields that shield the nucleus. Thus, the local magnetic field is different than the external applied magnetic field, as shown in the following equation:

$$B_{loc} = B(1-\sigma) \quad (3)$$

where σ is the shielding constant, providing the electron density around the nucleus.

NMR spectroscopy exploits the non-zero nuclear spin of isotopes, such as ^{1}H and ^{13}C, which have an odd number or protons and/or neutrons. ^{1}H NMR is the most used method of NMR technique for the study of polymers, that interacts with ^{1}H hydrogen nucleus. A constant magnetic field is initially applied, in order to align the magnetic nuclear spins of hydrogen atoms. A radio-frequency pulse, proportional to the constant magnetic field is utilized then to break the aligned nuclear spins. The final signal of NMR technique refers to the nuclei's intrinsic magnetic moment transition.

The resulting spectrum is the chemical shift (peaks) of the hydrogen nucleus resonant frequency in comparison with a reference sample of tetramethylosiloxane ($Si(CH_3)_4$, TMS) and is obtained in terms of part per million. Chemical shift δ is defined as:

$$\delta = (B_\alpha - B_\delta) / B_\alpha \times 10^6 \text{ ppm} \quad (4)$$

$$\delta = (\nu_\alpha - \nu_\delta) / \nu_\alpha \times 10^6 \text{ ppm} \quad (5)$$

where B_α and B_δ are the nuclei resonant magnetic fields of reference and measuring sample respectively, while ν_α and ν_δ are the nuclei resonance frequencies for reference and measuring sample respectively. The resonance of a shielded nucleus (high σ value) will be achieved in higher magnetic fields and lower frequencies.

The NMR spectrum can provide important information as the position of each chemical shift is characteristic for every nucleus and its environment. Also, the area underneath each peak

is proportional to the number of nucleus present in the sample. Last, but not least, the width of every peak can provide certain information about the nature of the specific nucleus.[75, 76]

Size-Exclusion Chromatography

This is a classic separation method for obtaining molecular weights and their relative distribution, along with the purity of polymers. The technique utilizes a low-concentration polymer solution that passes through columns comprised of a scaling-porous-size material and is separated based on the hydrodynamic volume of its molecular species. Small-sized molecules can infiltrate in the pores, travelling longer distance and thus are eluted last, while bigger-sized molecules travel smaller distance and thus are eluted first. The detection of the molecular species can be achieved utilizing multiple detectors, such as Refractive index and UV detectors. The use of proper narrow standards polymers is of great importance for the calibration of this method, in order to achieve the identification of both homopolymers and copolymers.

The resulting chromatogram can provide information about molecular weight distribution, elution time and volume, and homogeneity of the polymeric chains, while certain calculations can deliver details about molecular weight of the polymeric chains. The Number Average Molecular Weight is calculated using the following:

$$<M_n> = \frac{\sum Fi\,(ui)Mi}{\sum Fi\,ui} \quad (6)$$

where F(u) is the signal function in terms of elution time, and $F_i(u_i)$ the average height of area i and M_i the corresponding molecular weight that is calculated by the reference curve for u_i elution time.[77]

The Weight Average Molecular Weight is calculated using:

$$<M_w> = \frac{\sum Fi\,(u_i)Mi^2}{\sum Fi\,uiMi} \quad (7)$$

and the corresponding Molecular Weight Polydispersity is given by:

$$I = \frac{<M_w>}{<M_n>} \quad (8)$$

Dynamic Light Scattering (DLS)

Dynamic light scattering (DLS) is a characterization technique based on the Brownian motion of particles in a colloidal dispersion to calculate their size and size-distribution. Brownian motion refers to the random motion of particles in a colloidal dispersion due to thermal energy they obtain from collisions with the solvent's molecules. The bigger the particles, the slower the Brownian motion. Temperature and viscosity of the medium are necessary parameters for the technique. DLS utilizes a monochromatic laser light beam that scatters on a colloidal dispersion solution due to density fluctuations and measures the frequency difference over time between the incident and the scattered beam and can be described by the autocorrelation function:

$$G(t) = \langle I(0)I(t)\rangle = A + B\exp(-\Gamma t) = A + B\exp(Dq^2 t) \quad (9)$$

where A and B are constants, Γ is the, D is the diffusion coefficient and q is the scattering vector. The diffusion coefficient D is inversely proportional to the polymer's hydrodynamic radius, as depicted in the following equation:

$$D_0 = kT / 6\pi\eta R_h \quad (10)$$

where k is the Boltzmann constant, T is the absolute temperature, η refers to the solution viscosity and R_h is the hydrodynamic radius.

By studying intensity micro-differentiations of the scattered light beam by a polymeric solution as a function of time, one can calculate the polymer's hydrodynamic radius. In order to do so, a 2nd or 3rd degree polynomial is utilized to calculate the 1st and the 2nd cumulant, which refer to diffusion coefficient and size-distribution of the system respectively. Another method of R_h calculation is the CONTIN analysis, in which a number of solutions is given for the autocorrelation function regarding size distribution in the sample.[78]

Electrophoretic Light Scattering (ELS)

Electrophoretic Light Scattering is a scattering technique based on dynamic light scattering and is utilized for studying the electrophoretic mobility of colloidal particles and their zeta potential and surface charge in the presence of an applied electric field. The electrophoretic mobility is given by the following equation:

$$\mu = u/E = \varepsilon_r \varepsilon_0 \zeta / \eta \quad (11)$$

where u is the drift velocity of the dispersed particles and E the electric field strength, ε_r the dielectric constant of the dispersion medium, ε_0 the permittivity of free space, η the dynamic viscosity and ζ the zeta potential.

The method utilizes a laser beam of λ = 660 nm and 35 mW power. The beam separator divides both the incident and reference rays. A system of electrodes produces an external electric field inside the sample cell. The modulator keeps the reference and scattered beam frequencies in the same scale and a beam splicer combines them at 15°. Lastly, the detector provides the final data to a computer system for further analysis.[79]

Fluorescence Spectroscopy

Fluorescence spectroscopy is a characterization technique based on the physical phenomenon called luminescence, meaning the excitement of a certain molecule by light absorbance, followed by light emission during excitation relaxation. This phenomenon can be also addressed as fluorescence if the emission occurs 10^{-9}-10^{-6} seconds, or phosphorescent if the emission occurs 10^{-4}-10 seconds after the excitement, respectively.

The absorbance of either UV or visible light from a certain molecule leads to electron transition from bonding (π) or non-bonding (η) to anti-bonding (π*) orbitals and thus transitions from the ground electron state S_0 to one of the vibrational states of the first excited electron state S_1. The transition to the relaxed electron state occurs via 2 different intersystem conversion procedures. The first one refers to the vibrational relaxation in which all the excited vibrational states of the excited electron state return to the lowest vibrational state of the ground electron state. The second one is comprised of two phases. Initially, the relaxation from the lowest vibrational state of the excited electron state to the highest vibrational state of the

ground electron state occurs. The final phase results to the lowest vibrational state of the ground electron state for all electrons.

Fluorescence spectroscopy is of great importance, due to the ability of the fluorophores to interact with neighboring molecules, resulting in rich information about nano and microenvironment of the under-study sample. Fluorescent spectroscopy with pyrene is a characteristic method to examine the micropolarity of self-assembled polymeric systems. Pyrene is an extremely hydrophobic and fluorescent molecule and when injected to a colloidal dispersion system tends to avoid water. The resulting spectrum provides certain information of the micropolarity of the system by obtaining the I_1/I_3 peaks ratio of the pyrene fluorescence spectrum and is used to identify the existence of hydrophilic and/or hydrophobic domains inside the polymeric system, since this ratio depends on the polarity of the surroundings.[80]

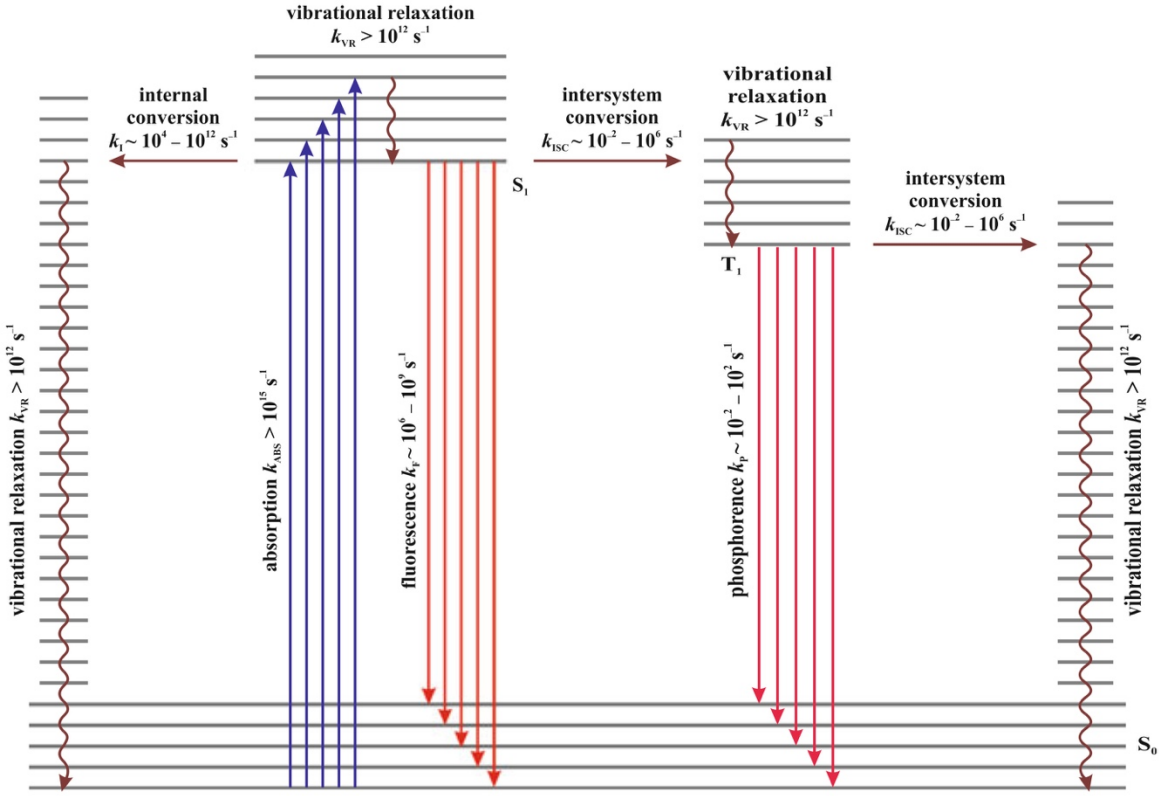

Figure 21: Jablonski diagram of the ground (S_0) and excited (S_1) electron state vibrational energies, along with the intermediate triplet (T_1) electron state.[80]

UV-Vis Spectroscopy

UV-Vis spectroscopy is a characterization technique based on the light absorbance ability of some materials and substances. The method measures either the Transmittance (T), or the Absorbance (A) of a solution placed in a cell, using the Beer-Lambert law:

$$A = -\log T = \log\frac{P_o}{P} = \varepsilon bc \quad (12)$$

where b is the optical route, c is the solution concentration, ε the molar attenuation coefficient, P and P_o the intensities of the incident and outbound beam respectively. The beam intensity should be equal for both sample and neat solvent in order to fix certain reflection issues occurring in the sample cell. Transmittance and Absorbance values are calculated by the following equations:

$$T = P/P_o \quad (13)$$

$$A = \log(P_o/P) \quad (14)$$

where P_o and P_o the beam intensities before and after transition through the sample cell.[81]

MATERIALS AND METHODS

DMAEMA (97%) and SMA (97%) monomers (obtained from Sigma Aldrich) were purified through columns filled with inhibitor removers (obtained from Sigma Aldrich). DMPC lipid (obtained from Sigma Aldrich) was used as received. AIBN was used as the radical initiator after recrystallization from methanol. 1,4-dioxane (98%, obtained from Sigma Aldrich) was dried over molecular sieves before use. Chloroform, PBS and other reagents (obtained from Sigma Aldrich) were used as received.

P(DMAEMA-*co*-SMA) Synthesis

Free-radical polymerization was utilized for the synthesis of DMAEMA-*co*-PSMA copolymers and a typical synthetic route is as follows: DMAEMA (2 g, mmol), SMA (0.2 g, mmol), AIBN (65.7 g), and 1,4-dioxane (10 mL, 30% w/w monomer concentration) were added in a round bottom flask (25 mL) equipped with a rubber septum. The solution was degassed for 15 minutes by high purity nitrogen gas, was left for 24 h at 70^{o}C, and terminated after quenching at -20^{o}C for 10 minutes and by exposure to air. The PDMAEMA-*co*-PSMA copolymers were precipitated in excess n-hexane for removal of unreacted monomers and were placed in a vacuum oven for 48 h for drying (yield 90%).

DMPC:P(DMAEMA-*co*-SMA) Hybrid Liposomes Preparation

A typical preparation of the Hybrid Liposomes is as follows: DMPC (0,03g, mmol), PDMAEMA-*co*-PSMA (g, mmol) and chloroform were added in a round flask (100 mL). The mixture was placed into a rotor evaporator, at 30^{o}C aqueous bath for 60 minutes under vacuum, until complete evaporation of chloroform. The formed DMPC:PDMAEMA-*co*-PSMA thin film was stored at 2^{o}C for 24 h. The thin film hydration was achieved using PBS aqueous solution, followed by a double 5-minute probe sonication.

Self-Assembly Studies

Direct solubilization in PBS was used initially for the preparation of PDMAEMA-*co*-PSMA and DMPC:PDMAEMA-co-PSMA stock solutions. Then, the stock solutions were regulated into two different pH values (pH 3, 7) by addition of appropriate amounts of 1 M solutions of HCl.

Drug Loading Studies

DMPC:PDMAEMA-*co*-PSMA/Curcumin samples were prepared by thin film protocol and hydration in PBS, followed by a double 5-minute tip sonication. Curcumin quantity was calculated as of 10 and 20% w/w of the total DMPC:PDMAEMA-*co*-PSMA mass in each case.

Methods

Size-exclusion chromatography (SEC) was utilized for molecular weights and molecular weight distributions of the random copolymers. The SEC system was consisted of a Waters 1515 isocratic pump, three μ-Styragel mixed bed columns (10^2-10^6 Å) and a Waters 2414 refractive index detector (at 40^{o}C) all controlled through Breeze software. The mobile phase was THF (containing 5% v/v triethylamine) and the flow rate was 1.0 mL/min at 30^{o}C. The SEC system was calibrated by using linear polystyrene standards with narrow polydispersities and molecular weights from 1200 to 929,000 g/mol.

^{1}H NMR spectroscopy was utilized to evaluate the random copolymers synthesis, along with the quantification of each monomer composition. The ^{1}H NMR spectra were obtained by a Bruker AC 300 FT-NMR spectrometer (300 MHz). The samples were dissolved in deuterated chloroform ($CDCl_3$). The spectra were taken in parts per million (ppm) relative to tetramethylsilane (TMS).

PDMAEMA-*co*-PSMA: ^{1}H NMR [Fig., 300 MHz, Acetone d_6, 2.04 ppm]: 3.90 (2H, –COO*CH*$_2$(CH_2)$_{16}$$CH_3$–), 2.60 (2H, –O$CH_2$*CH*$_2$N($CH_3$)$_2$–), 2.35 (6H, –NH*(CH*$_3$*)*$_2$–), 1.80 (2H, –*CH*$_2$C–), 1.17 (32H, –*CH*$_2$*(CH*$_2$*)*$_{16}$$CH_3$–), 0.65 (3H, –$CH_2$C*CH*$_3$–, 3H –$CH_2$($CH_2$)$_{16}$*CH*$_3$–).

Dynamic light scattering technique was utilized to determinate the nanoparticles' size, along with their size distribution in aqueous solutions. Measurements were conducted on a ALVGmbH system, with an ALV/CGS-3 compact goniometer, an ALV 5000/EPP multi-τ digital correlator with 288 channels and an ALV/LSE-5003 light scattering electronics unit for stepper motor drive and limit switch control. The light source was a JDS Uniphase 22 mW He-Ne lase (λ=632.8 nm). The temperature of the measurement cell was controlled through a Polyscience 9102A12E bath circulator. Five measurements were taken at each angle, which were averaged. The correlation function analysis was performed by the cumulant methods, as well

as the CONTIN software. Static light scattering measurements were conducted on the same equipment in the angular range of 30-150^{o}. The calibration standard was toluene and data were analyzed by Zimm and Guinier methods.

FTIR measurements were conducted on an Equinox 55, Bruker Optics system equipped with a single reflection diamond ATR accessory (Dura-Sam-p1IR II by SensIR Technologies) in the region of 550-4000 cm^{-1}.

P(DMAEMA-co-SMA): FTIR: v = 2853 (s), 1728 (s), 1468 (s), 1147 (s) cm^{-1}

A ZetaSizer Nano series Nano-ZS (Malvern Instruments Ltd, Malvern, UK), utilizing a He-Ne laser beam at 633 nm at a fixed backscattering angle of 173^{o} was used for Electrophoretic light scattering measurements. The Henry correction of the Smoluchowski equation was used for data analysis, after equilibration at 25^{o}C. Zeta-potential (ζ_p) values were taken as the average of 50 runs.

Fluorescence spectra were recorded on a Fluorolog-3 Jobin Yvon-Spex spectrofluoremeter (model GL3-21). The excitation wavelength was nm and the fluorescence spectra were collected in the range of nm. No excimer formation was observed for the copolymer solutions.

UV-vis spectra were recorded on a Perkin-Elmer (Lambda 19) UV-Vis-NIR spectrofluoremeter, using 3 mL of the sample inside a quartz cell.

RESULTS

Synthesis of P(DMAEMA-*co*-SMA) copolymers

Two PDMAEMA-*co*-PMSA copolymers were synthesized using free-radical polymerization, as shown in Fig. 22. Molecular characterization of the random copolymers was conducted utilizing SEC, NMR and FTIR techniques. SEC chromatogram shows the successful synthesis of the random copolymers by showing a very broad double-peak, depicting the large molecular polydispersity of the synthesized random copolymers (Fig. 23). Characteristic peaks of both DMAEMA (2.3 ppm) and SMA (1.1 ppm) can be identified from the NMR spectra (Fig) and quantify the composition of each monomer. FTIR spectrum also proves the successful synthesis by showing the qualitative existence of characteristic peaks corresponding to each monomer in the copolymer (Fig. 23).

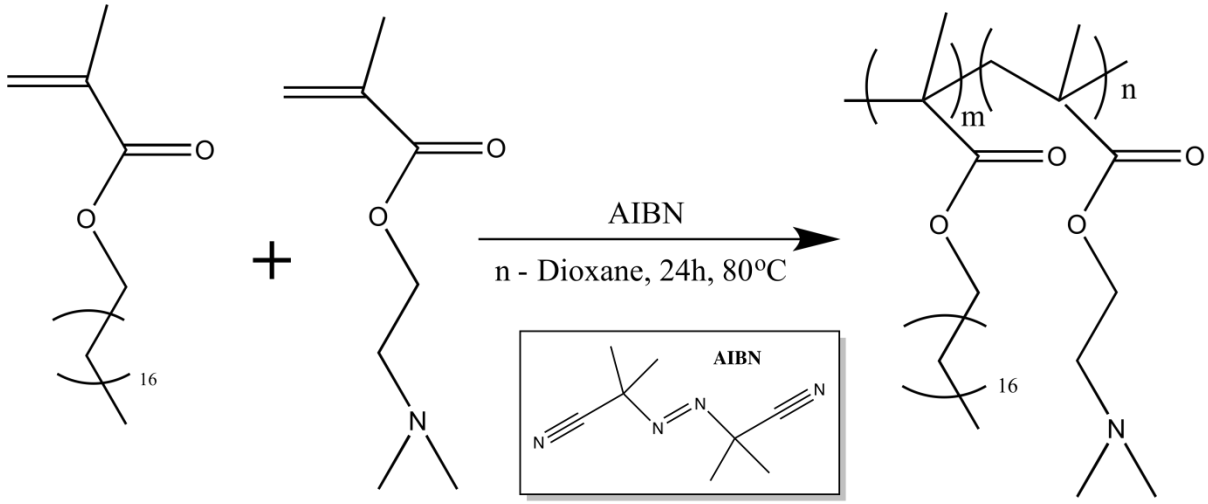

Figure 22: *Synthetic route of P(DMAEMA-co-SMA) utilizing free-radical polymerization.*

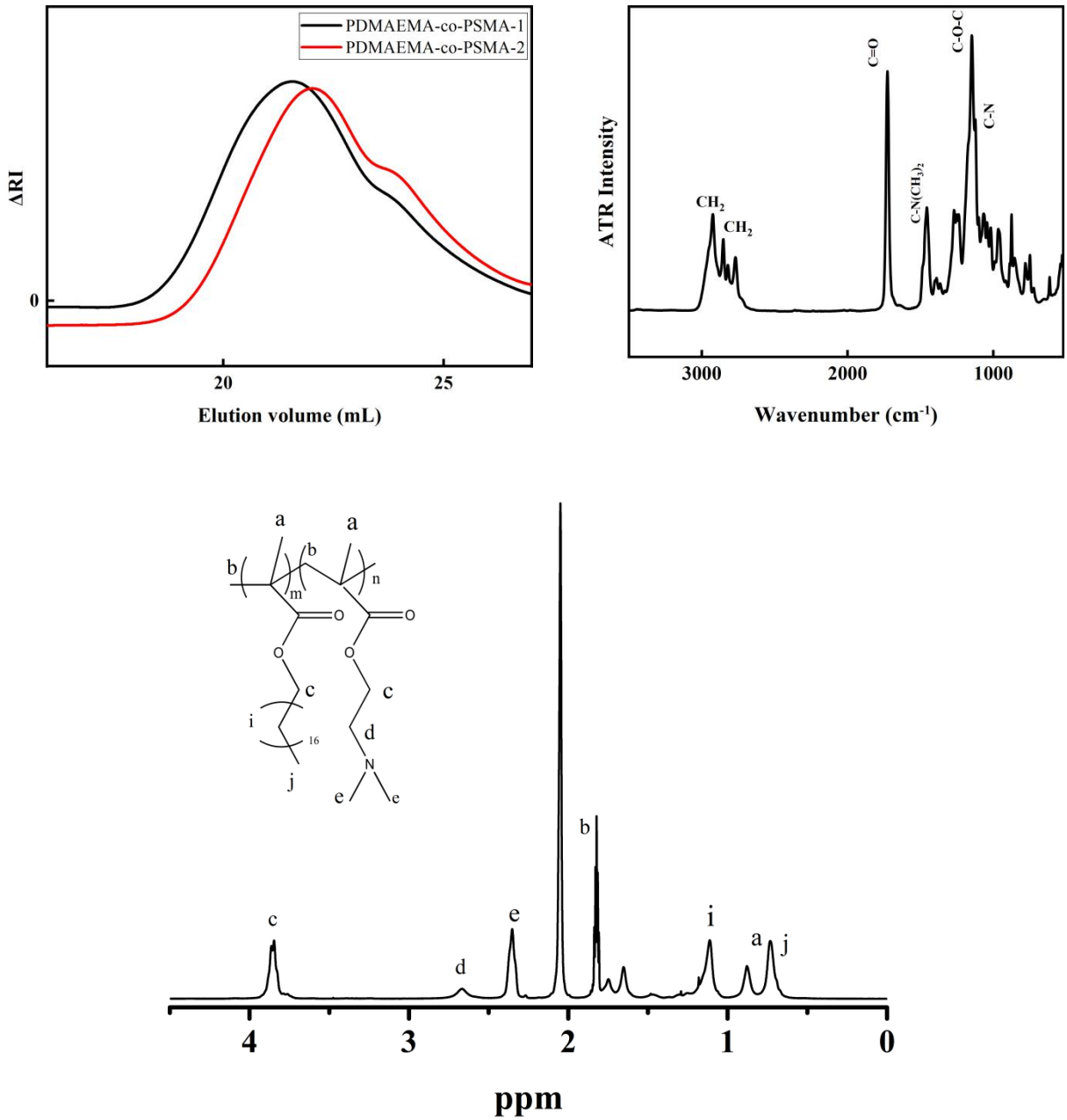

***Figure 23**: Size exclusion chromatogram (top left), ATR-FTIR spectrum (top right) and NMR spectrum (bottom) of P(DMAEMA-co-SMA).*

Results in Table 1 show large molecular weights and rather large molecular weight polydispersities, confirmed by SEC chromatograms (Fig. 23) which show double and broad peaks for both random copolymers, indicating large molecular weight polydispersities, which is acceptable for this study and in line with free radical polymerization methodology. This is rather acceptable for this kind of polymerization, since there is no control of the radicals and thus completely random (statistical) copolymers are synthesized via this way.

Table 1: *Molecular weights and their polydispersity along with monomer composition.*

Sample	M_w (g/mol)[a]	M_w/M_n[a]	% PDMAEMA[b]	% PSMA[b]
P(DMAEMA-*co*-SMA)-1	71100	2.9	90	10
P(DMAEMA-*co*-SMA)-2	50000	3.4	70	33

[a]Determined by SEC
[b]Determined by ^{1}H NMR

Aqueous Solution Studies on P(DMAEMA-*co*-SMA)

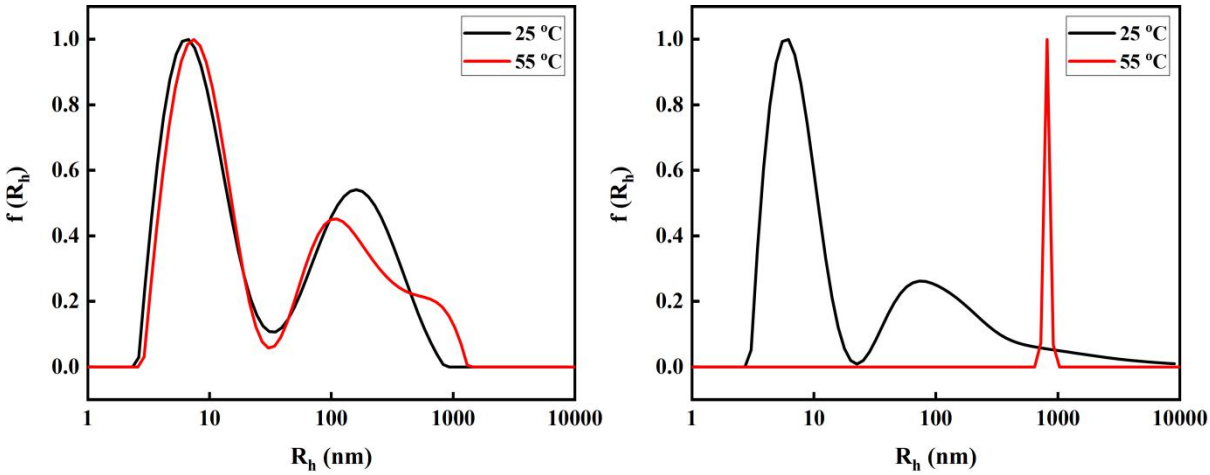

***Figure 24**: CONTIN analysis P(DMAEMA-co-SMA)-1 for pH 3 (left) and pH7 (right) aqueous solutions.*

Aqueous solution studies on both random copolymers were conducted in PBS, at pH 3 and pH 7, since PDMAEMA is pH-responsive. CONTIN analysis graphs for P(DMAEMA-*co*-SMA)-*1* at pH 3 and pH 7 present two large-polydispersed size-populations, at 9 and 230 nm (in pH 3) and 90 nm (in pH 7), depicting the formation of unimers and aggregates, respectively. In the case of pH 3 the size populations are unaffected by the temperature increase at 55°C, while at pH 7 the two populations form a new single, well-defined size-population at 900 nm, due to the thermo-responsive character of PDAEMA, depicting the formation of large, multicompartment aggregates (Fig. 24).

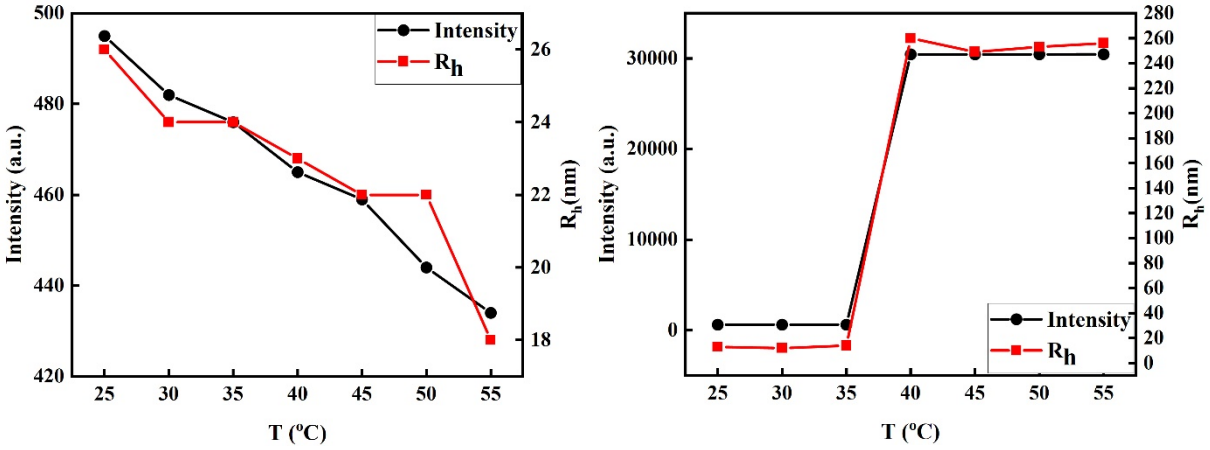

***Figure 25**: Average Intensity and R_h values as a function of temperature for P(DMAEMA-co-SMA)-1 at pH 3 (left) and pH 7 (right).*

The average intensity and R_h values for P(DMAEMA-*co*-SMA)-*1* in aqueous solutions of pH 3 show rather small changes as a function of temperature, while at pH 7 there is a sharp transition after 35°C, depicting the thermo-responsive behavior of PDMAEMA (Fig. 25).

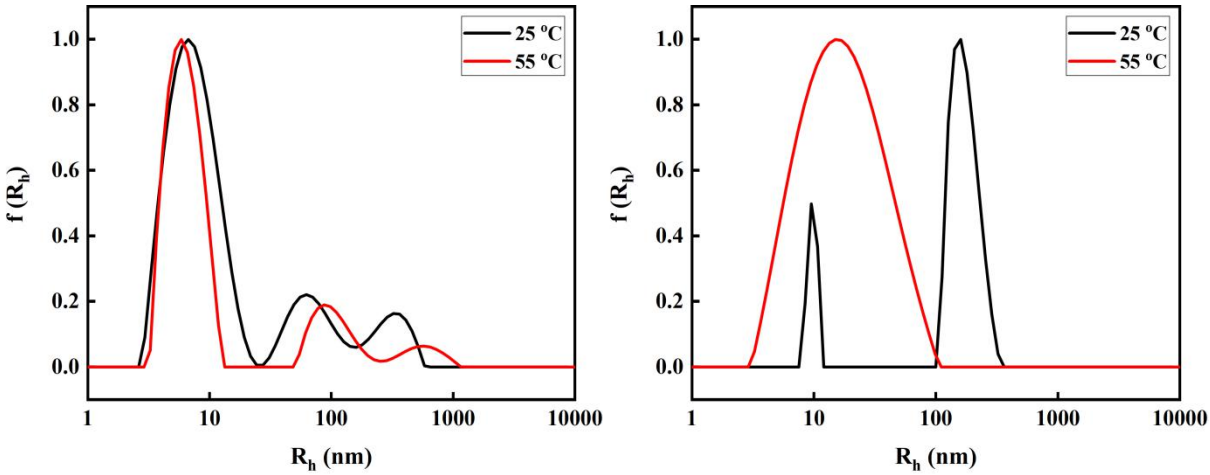

***Figure 26**: CONTIN analysis P(DMAEMA-co-SMA)-2 for pH 3 (left) and pH7 (right) aqueous solutions.*

DLS measurements on P(DMAEMA-*co*-SMA)-*2* show the existence of 3 size-populations at pH 3, at 8, 90 and 500 nm respectively, which mostly remain unaffected by temperature increase. CONTIN analysis graphs at pH 7 show two, well-defined size-populations at 9 and 200 nm, again depicting the existence of unimers and aggregates respectively, while a rise in temperature leads to the formation of one, single, large-dispersity size-population at 30 nm. This probably depicts the removal of water from the aggregates' core, and/or the breakage of larger aggregates and the formation of new, smaller ones (Fig. 26).

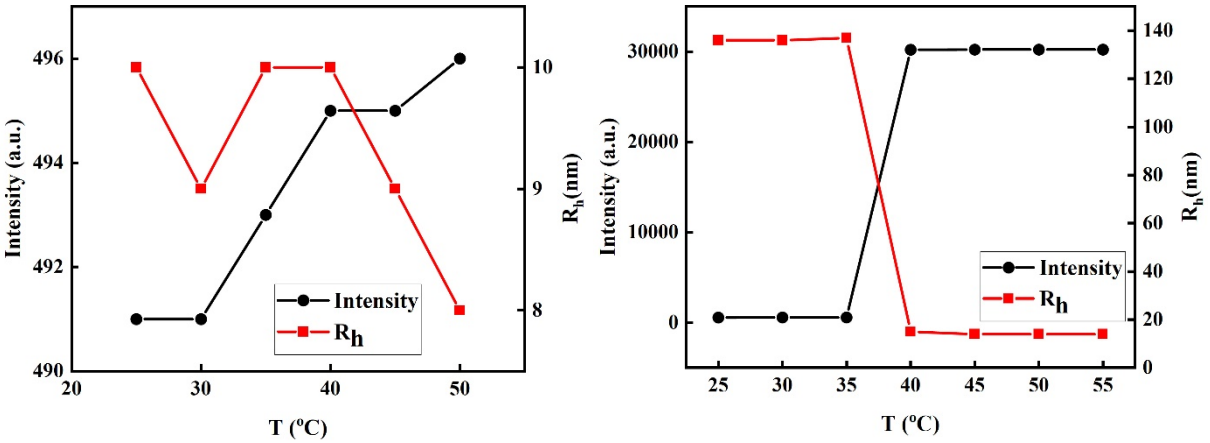

***Figure 27**: Average Intensity and R_h values as a function of temperature for P(DMAEMA-co-SMA)-2 at pH 3 (left) and pH 7 (right).*

Figure 27 shows that the average values of both intensity and R_h for P(DMAEMA-*co*-SMA)-*2* show insignificant changes in pH 3 aqueous solutions as a function of temperature. On the

other hand, aqueous solution studies on pH 7 show the thermo-responsive behavior of PDMAEMA after 35^{o}C, presenting a sharp transition for both values, only this time the average R_h is reduced from 140 to 12 nm. Combined with the sudden increase of average intensity, leads to the conclusion that the system expels water from its cores, along with a great increase in mass.

Z-potential measurements at pH 3 and pH 7 aqueous solutions show positive surface charge, due to the presence of PDMAEMA, which becomes fully protonated at pH 3 and thus resulting in larger ζ-potential values. Fluorescence spectroscopy measurements were conducted via the use of pyrene, in order to investigate the micropolarity of the P(DMAEMA-*co*-SMA) copolymer nanostructures. The results show a drop in I_1/I_3 ratio values as the pH values increase, due to the fact that PDMAEMA becomes partially protonated at pH 7 and thus less hydrophilic. P(DMAEMA-*co*-PSMA)-2 presents extremely hydrophobic domains, probably due to the increased composition in SMA (33%).

Table 2: Surface charge and micropolarity studies of P(DMAEMA-co-SMA) copolymers in aqueous solutions.

Sample	pH	I_1/I_3	ζ-potential (mV)
P(DMAEMA-*co*-SMA)-1	3	1.21	35
P(DMAEMA-*co*-SMA)-1	7	1.03	4
P(DMAEMA-*co*-SMA)-2	3	0.95	38
P(DMAEMA-*co*-SMA)-2	7	0.94	7

Preparation of DMPC:P(DMAEMA-co-SMA) Hybrid/Chimeric Liposomes

Four chimeric/hybrid liposome systems with various phospholipids/copolymers molar ratios were prepared as shown in Table 3. Since the molecular weights of both random copolymers were large, molecular ratios of 0.02 and 0.1 were preferred, in order to avoid the lipid bilayer rupture due to the presence of the copolymer. Preparation was carried out via thin-film protocol, hydration and tip sonication.

Table 3: *DMPC:P(DMAEMA-co-SMA) Samples.*

Sample	Lipid:Copolymers ratio	DMPC	Copolymer
DMPC:P(DMAEMA-*co*-SMA)-*1*	9:0.02	60 mg	14 mg
DMPC:P(DMAEMA-*co*-SMA)-*1*	9:0.1	30 mg	36, 09 mg
DMPC:P(DMAEMA-*co*-SMA)-*2*	9:0.02	60 mg	9,8 mg
DMPC:P(DMAEMA-*co*-SMA)-*2*	9:0.1	60 mg	49 mg

Aqueous Solution Studies on DMPC:P(DMAEMA-*co*-SMA)

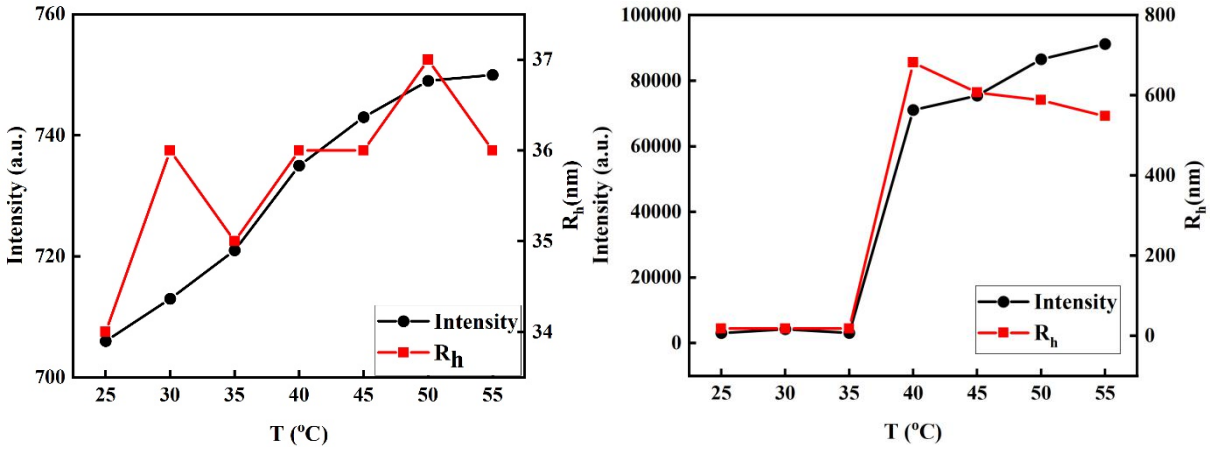

***Figure 28**: DLS results of average intensity and R_h of DMPC:P(DMAEMA-co-SMA)-1 1:0.02 in pH 3 (left) and pH 7 (right) aqueous solutions.*

DLS studies on DMPC:P(DMAEMA-*co*-SMA)-1, 1:0.02 show the formation of nanoparticles with an average R_h of 34 and 19 nm for pH 3 and pH 7 aqueous solutions respectively. Extremely low average intensity values depict the low mass of the formed nanoparticles. Since PDMAEMA does not present thermo-responsive behavior at pH 3 there is no observable differentiation in the system, while a temperature increase at pH 7 leads to a sharp transition after 35°C on both intensity and R_h values, as shown in Fig. 28.

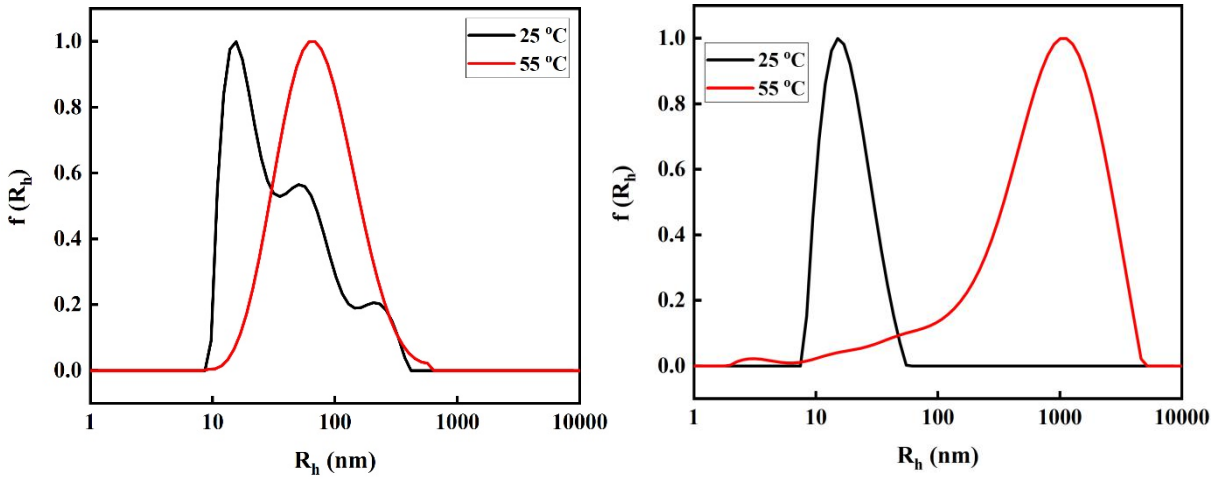

***Figure 29**: CONTIN analysis for DMPC:P(DMAEMA-co-SMA)-1 1:0.02 in pH 3 (left) and pH 7 (right) aqueous solutions at 25°C and 55°C.*

CONTIN analysis of DLS correlation functions for DMPC:P(DMAEMA-*co*-SMA)-1 1:0.02 in pH 3 aqueous solution show the formation of polydispersed nanoassemblies that are unaffected by temperature rise. On the other hand, pH 7 aqueous solutions present a rather well-defined

mono-dispersed system at 19 nm that is heavily aggregated at 55°C, due to the thermosensitive aggregation of PDMAEMA (Fig. 29). The specific system was not particularly stable, since the smallest dilution produced more than one size-populations.

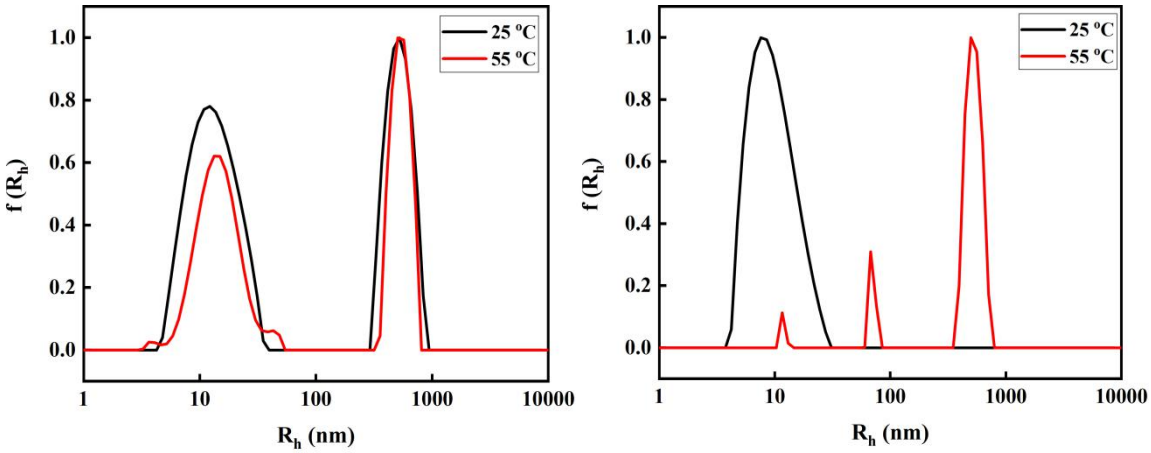

***Figure 30**: CONTIN analysis of DMPC:P(DMAEMA-co-SMA)-1 9:0.1 in pH 3 (left) and pH 7 (right) aqueous solutions at 25°C and 55°C.*

DMPC:P(DMAEMA-*co*-SMA)-1 9:0.1 samples at pH 3 form two distinct and well-defined size-populations at 11 and 900 nm respectively that do not present any thermo-responsiveness, as depicted on the CONTIN analysis of DLS correlation functions graphs (Fig. 30). The pH 7 aqueous solutions graphs show a single well-defined size population at 25°C, which turns into three, also well-defined size populations, at 11, 90 and 870 nm respectively upon temperature rise to 55°C.

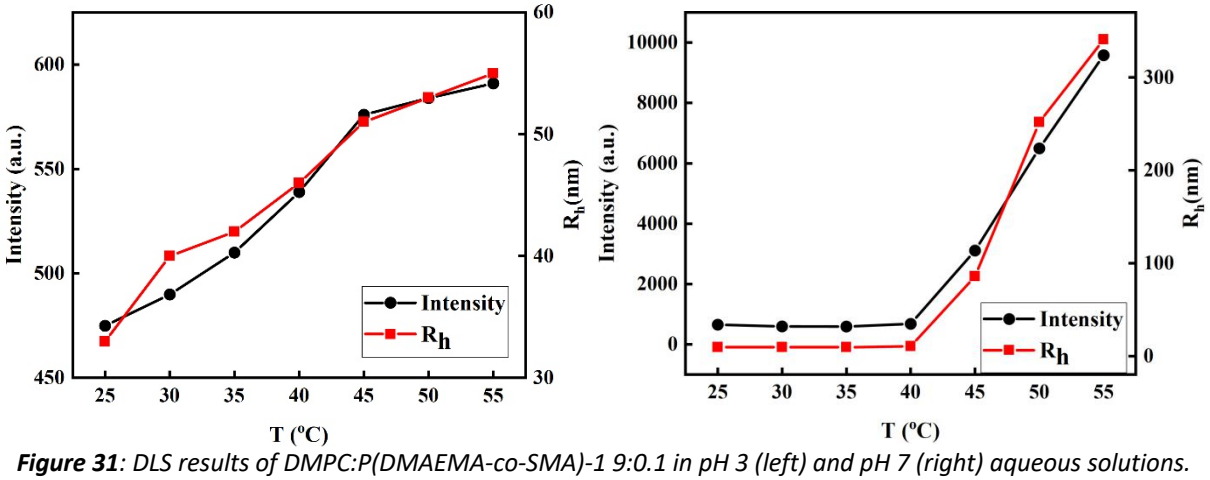

***Figure 31**: DLS results of DMPC:P(DMAEMA-co-SMA)-1 9:0.1 in pH 3 (left) and pH 7 (right) aqueous solutions.*

A more thorough investigation of the pH 7 aqueous solutions has been conducted, showing a 9 nm initial average R_h at 25°C, which increases linearly upon temperature rise after 40°C.

Average intensity values are low, depicting the low mass of the formed nanoassemblies, but presents a linear rise upon temperature increase after 40°C (Fig. 31).

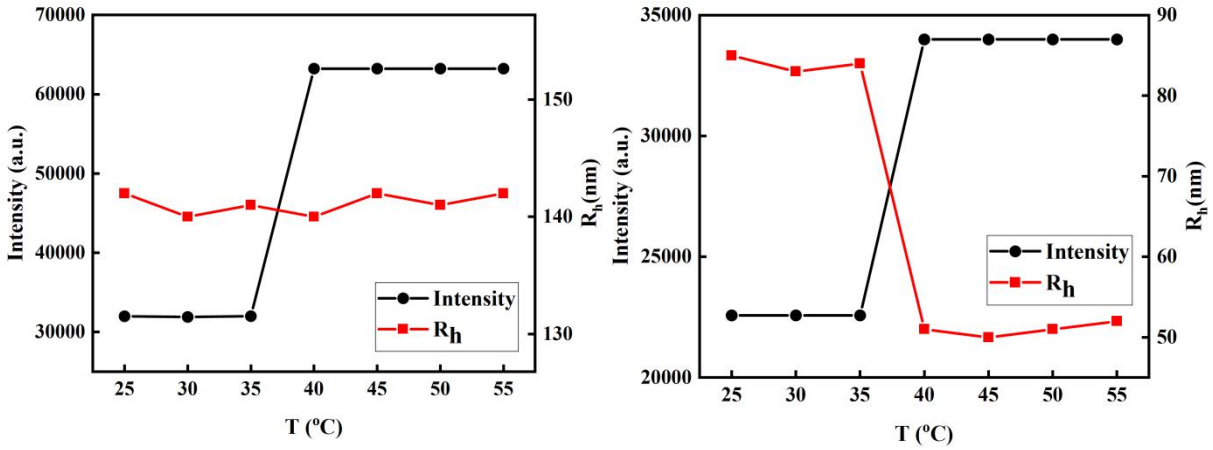

***Figure 32**: DLS results of DMPC:P(DMAEMA-co-SMA)-2 9:0.02 in pH 3 (left) and pH 7 (right) aqueous solutions.*

The P(DMAEMA-co-SMA)-2 random copolymer is comprised of 60% PDMAEMA and 40% PSMA and its incorporation inside DMPC liposomes results in larger hybrid nanoparticles. The second series of polymeric liposomes were measured with a 1:5 sample to PBS water ratio dilution, due to the high scattering intensity of the solution. Thus, the Intensity/R_h versus temperature graphs of the DMPC:P(DMAEMA-*co*-SMA)-2 9:0.02 samples in pH 3 aqueous solutions depicts the formation of nanoassemblies with a steady R_h of 142 nm at all temperatures, while intensity values produce a sudden transition after 35°C, depicting an increase in system's mass. pH 7 aqueous solutions of DMPC:P(DMAEMA-*co*-SMA)-2 9:0.02 show a sharp transition on both R_h and intensity values. More specifically, the system produces nanoassemblies with R_h of 85 nm, reduced to 53 nm after 35°C, while intensity values are increased, depicting the loss of absorbed water along with an increase of the mass of the nanosystem (Fig. 32).

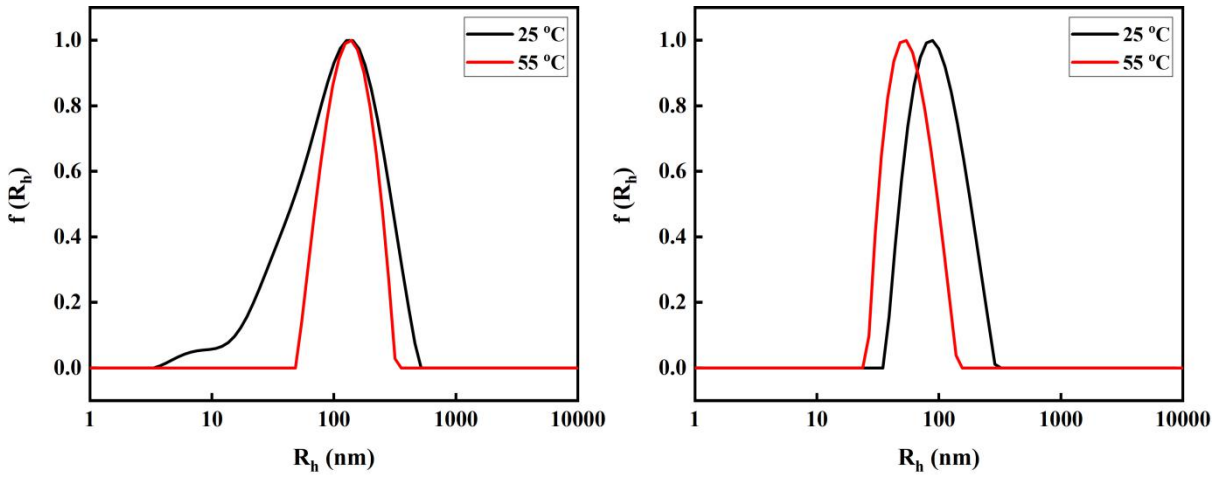

***Figure 33**: CONTIN analysis of DMPC:P(DMAEMA-co-SMA)-2 9:0.02 in pH 3 (left) and pH 7 (right) aqueous solutions at 25°C and 55°C.*

The DMPC:P(DMAEMA-co-SMA)-2 9:0.02 nanosystem forms a single polydispersed size population at 25°C at pH 3, which becomes more well-defined after temperature increase to 55°C. In the case of pH 7 aqueous solution, the system self-assembles into a single well-defined population at 25°C, while temperature increase to 55°C reduces the overall size (Fig. 33).

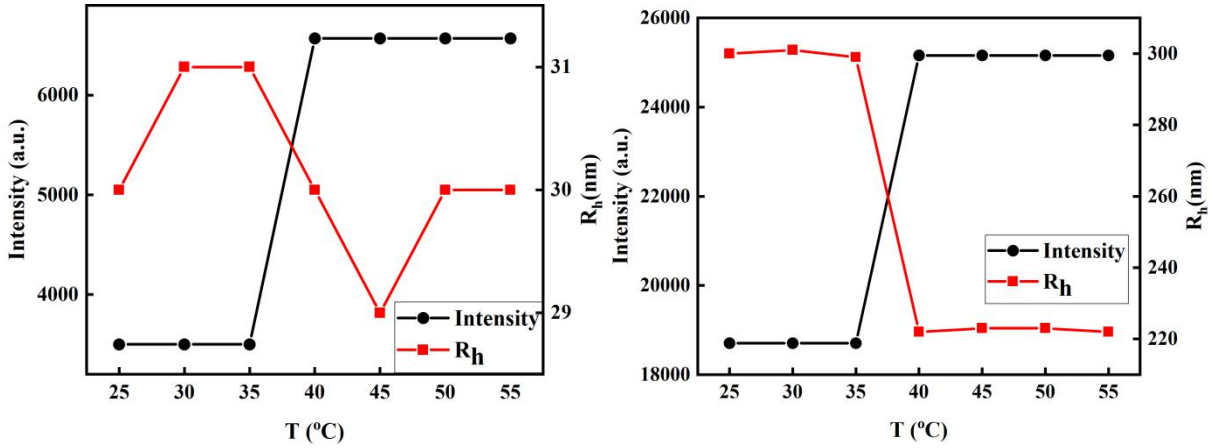

***Figure 34**: DLS results of DMPC:P(DMAEMA-co-SMA)-2 9:0.1 in pH 3 (left) and pH 7 (right) aqueous solutions.*

The final DMPC:P(DMAEMA-*co*-SMA)-2 sample with 9:0.1 molar ratio self-assembles in small nanoparticles of 30 nm R_h, which are unaffected by temperature changes. On the other hand, there is a sharp transition that doubles intensity values after 35°C, depicting a sudden change in the mass of the system. At pH 7, the system forms large nanoassemblies with an initial R_h of 300 nm at 25°C and high values of intensity. Increasing the temperature above 35°C, a sharp transition is observable for both R_h and temperature, depicting a mass-gain while removing water from the hydrophobic domains (Fig. 34).

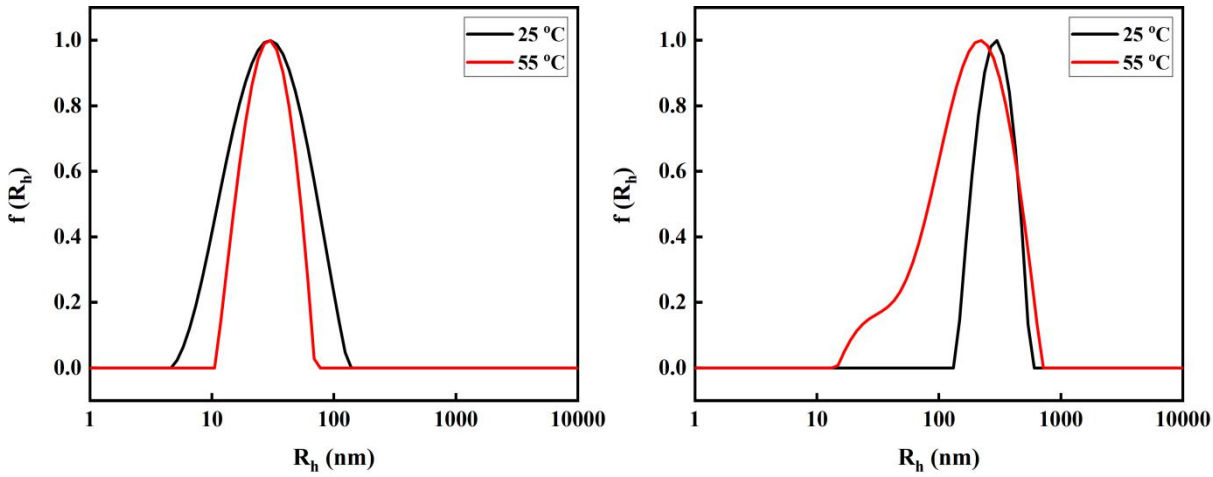

***Figure 35**: CONTIN analysis of DMPC:P(DMAEMA-co-SMA)-2 9:0.1 in pH 3 (left) and pH 7 (right) aqueous solutions at 25°C and 55°C.*

CONTIN analysis of the DLS correlation functions of the DMPC:P(DMAEMA-*co*-SMA)-2 9:0.1 for pH 3 presents a single, rather small but polydispersed size population at 25°C. Temperature increase does not affect the size of the formed nanoassemblies, but produces a better defined size population. The DMPC:P(DMAEMA-co-SMA)-2 0:0.1 system at pH 7 forms a rather large, but well-defined population. Heating above 35°C leads to R_h decrease along with a huge increase in size-distribution (Fig. 35).

Z-potential and Micro-Polarity Studies

Micropolarity studies were conducted utilizing fluorescence spectroscopy with the addition of pyrene in order to determine the hydrophobic character of each system. Pyrene is an extremely hydrophobic molecule, which tends to reside in hydrophobic domains. Since it is fluorescent, by conducting photoluminescence measurements, the resulting I_1/I_3 ratio provides useful information about the micro polarity of the system under study. I_1/I_3 ratio values are in the 0,97 to 1,1 range, indicating a strong presence of hydrophobic domains for all systems. Z-potential measurements depict positive surface charge values, ranging from 7 to 14 mV, depending the pH of the aqueous solution. Higher ζ-potential values at pH 3 confirm the presence of cationic PDMAEMA, since it is fully protonated and thus the chimeric nanoparticles exhibit higher surface charge.

***Table 4**: Surface Charge and Micropolarity Results of P(DMAEMA-co-SMA) and DMPC:P(DMAEMA-co-SMA) samples*

Sample	pH	Molar Ratio	I_1/I_3	ζ
P(DMAEMA-*co*-PSMA-1	3	-	1.21	35
P(DMAEMA-*co*-PSMA-1	7	-	1.03	4
P(DMAEMA-*co*-PSMA-2	3	-	0.95	38
P(DMAEMA-*co*-PSMA-2	7	-	0.94	7
DMPC:P(DMAEMA-*co*-SMA)-1	3	9:0.02	1,17	10
DMPC:P(DMAEMA-*co*-SMA)-1	7	9:0.02	1,11	7
DMPC:P(DMAEMA-*co*-SMA)-1	3	9:0.1	1,13	11
DMPC:P(DMAEMA-*co*-SMA)-1	7	9:0.1	1,08	8
DMPC:P(DMAEMA-*co*-SMA)-2	3	9:0.02	1	11
DMPC:P(DMAEMA-*co*-SMA)-2	7	9:0.02	0,995	9
DMPC:P(DMAEMA-*co*-SMA)-2	3	9:0.1	1	14
DMPC:P(DMAEMA-*co*-SMA)-2	7	9:0.1	0,97	9

Drug Loading on DMPC:P(DMAEMA-*co*-SMA). Curcumin as the model drug

Two DMPC:P(DMAEMA-*co*-SMA) systems were chosen for drug-loading with curcumin, since they are the most stable and present the most preferable characteristics. Curcumin loading was mediated through the thin film deposition and hydration process, followed by a double 5-minute tip-sonication. Four curcumin-loaded DMPC-P(DMAEMA-*co*-SMA) samples were prepared, as depicted in Table 5, but only the ones with 10% w/w curcumin were stable enough to proceed to further characterization.

***Table 5**: Drug-loading calculations for DMPC:PDMAEMA-co-PSMA hybrid/chimeric systems*

Sample	Molar Ratio	DMPC	P(DMAEMA-*co*-SMA)	Curcumin	Curcumin w/w %
DMPC:P(DMAEMA-co-SMA)-1	9:0.1	30 mg	36,09 mg	6,6 mg	10%
DMPC:P(DMAEMA-*co*-SMA)-1	9:0.1	30 mg	36,09 mg	13,2 mg	20%
DMPC:P(DMAEMA-*co*-SMA)-2	9:0.02	60 mg	9,8 mg	6,98 mg	10%
DMPC:P(DMAEMA-*co*-SMA)-2	9:0.02	60 mg	9,8 mg	13,96 mg	20%

Aqueous Solution Studies on DMPC:P(DMAEMA-*co*-SMA)/Curcumin

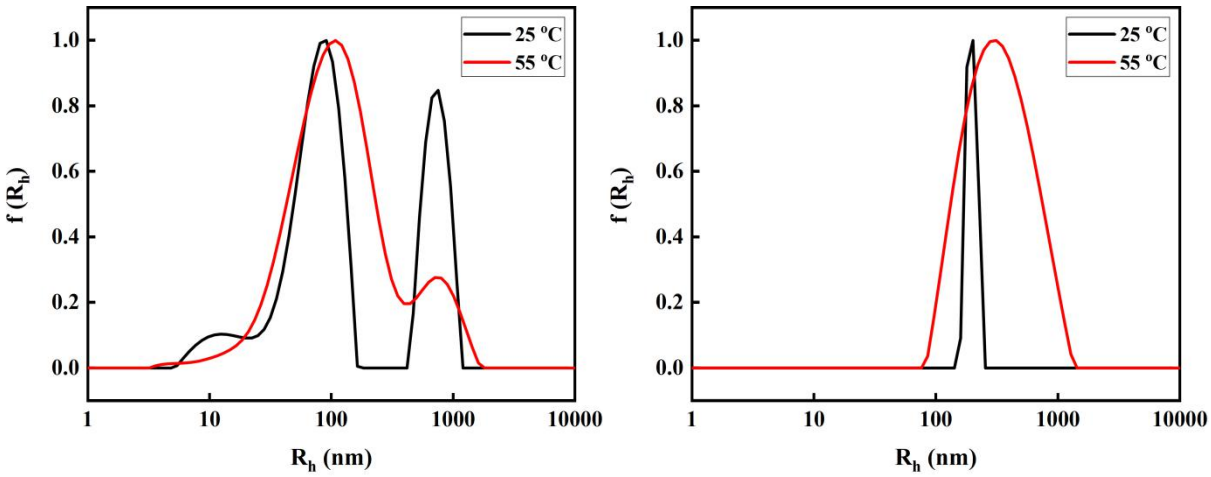

***Figure 36**: CONTIN analysis of DMPC:P(DMAEMA-co-SMA)-1 9:0.1 Curcumin 10% in pH 3 (left) and pH 7 (right) aqueous solutions at 25°C and 55°C.*

DLS studies were conducted on 10% w/w curcumin-loaded DMPC:P(DMAEMA-*co*-SMA)-1 9:0.1 samples at both pH 3 and pH 7 values. CONTIN analysis of the DLS correlation functions on pH 3 aqueous solution showed the existence of one polydispersed size population with nanoparticles of R_h around 90 nm and one well-defined size population referring to aggregates, with R_h values at 900 nm at 25°C. Temperature rise to 55°C affects the system by forming large polydispersed and non-distinct size populations. On the other hand, the pH 7 aqueous solutions present a single, very well-defined size population at 226 nm at 25°C, which turns broader, while increasing to 668 nm upon heating to 55°C. It is rather important to mention that the specific curcumin-loaded samples were extremely stable, even after 3 months' time passage after their preparation (Fig. 36).

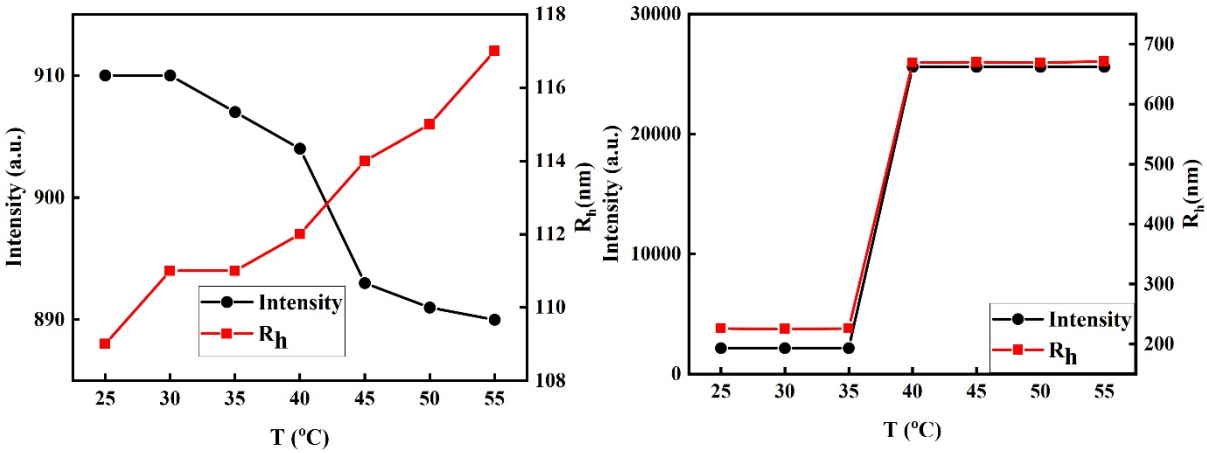

***Figure 37**: DLS study of DMPC:P(DMAEMA-co-SMA)-1 9:0.1 Curcumin 10% in pH 3 (left) and pH 7 (right) aqueous solutions.*

The average intensity and R_h values of DMPC:P(DMAEMA-*co*-SMA)-1 9:0.1 Curcumin 10% in pH 3 aqueous solutions present small changes as a function of temperature, probably due to hydrophobic interactions. pH 7 aqueous solutions show a sharp transition for both average intensity and R_h values after 35°C, depicting the thermo-responsiveness of the system, coming from the DMAEMA segments (Fig. 37).

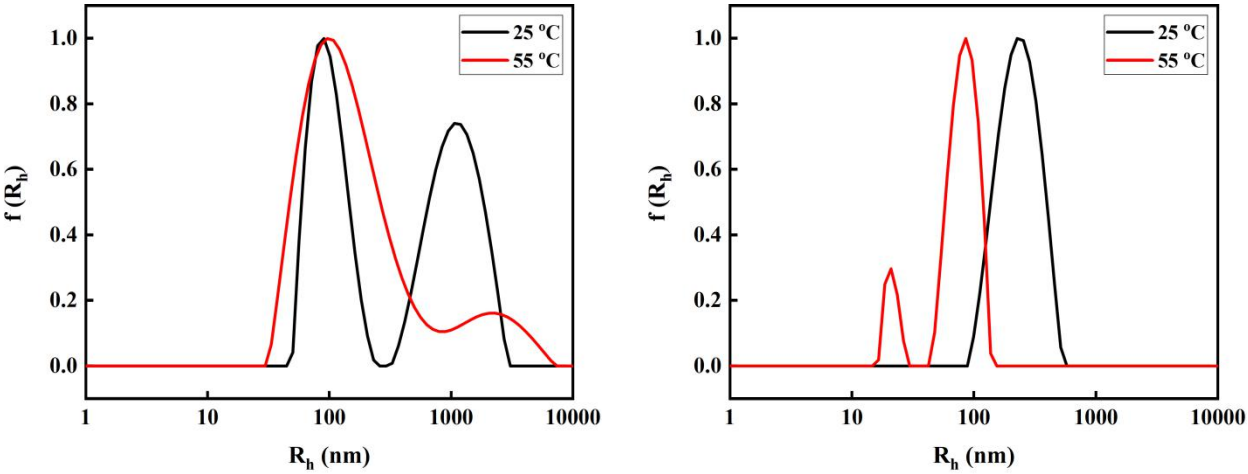

***Figure 38**: CONTIN analysis of DMPC:P(DMAEMA-co-SMA)-2 9:0.02 Curcumin 10% w/w in pH 3 (left) and pH 7 (right) aqueous solutions at 25°C and 55°C.*

The same DLS measurement procedure was followed for the 10% w/w the curcumin-loaded DMPC:P(DMAEMA-*co*-SMA)-2 9:0.02 samples. CONTIN analysis of the DLS correlation functions on pH 3 aqueous solutions at 25°C showed the existence of two distinct size populations, at 90 and 1000 nm respectively, depicting the presence of both nanoparticles and aggregates, while further temperature increase to 55°C lead to one large polydispersed size-population. The system in pH 7 aqueous solution at 25°C forms a single and very well-

defined size population at 200 nm, which is affected by temperature increase, resulting in a large-polydispersed size-population at 55°C (Fig. 38).

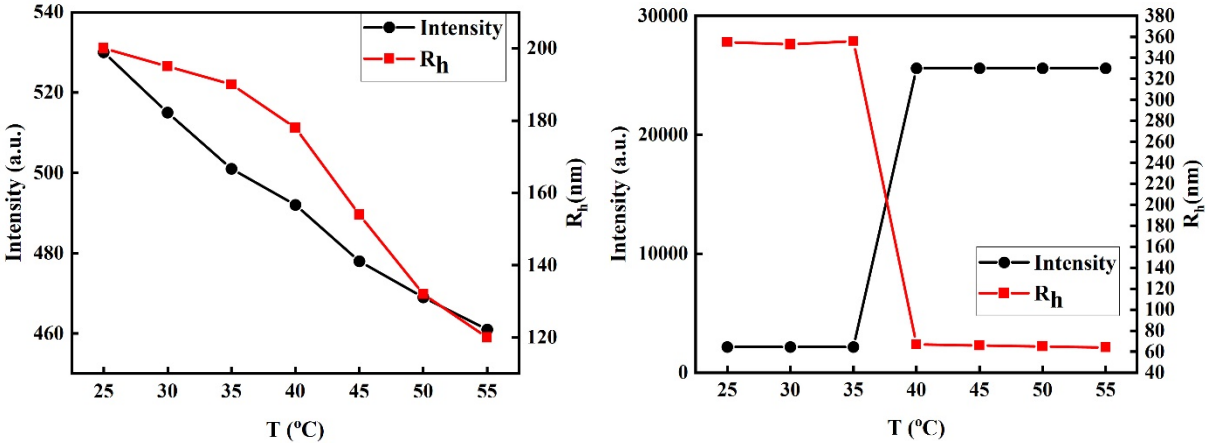

***Figure 39**: DLS study of DMPC:P(DMAEMA-co-SMA)-2 9:0.02 Curcumin 10% in pH 3 (left) and pH 7 (right) aqueous solutions.*

The average values of intensity and R_h of the DMPC:P(DMAEMA-*co*-SMA)-2 9:0.02 samples are decreasing as a function of temperature in aqueous solutions of pH 3, probably due to hydrophobic interactions. In pH 7 aqueous solutions, the system presents a sharp transition after 35°C giving very high values of average intensity, while at the same time average R_h values decrease from 360 to 64 nm (Fig. 39). This is a typical water expelling procedure, with a simultaneous increase in mass, depicting the thermo-responsive behavior of the system coming from DMAEMA segments.

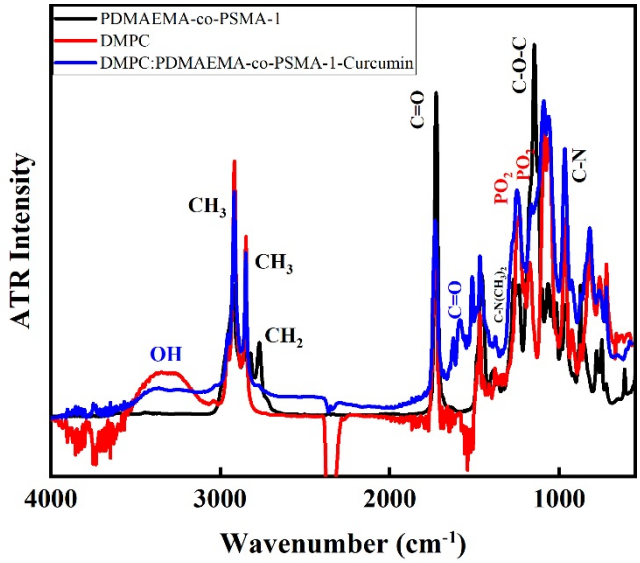

***Figure 40**: ATR-FTIR comparison spectra of P(DMAEMA-co-SMA)-1 (black line), DMPC (red line) and DMPC:P(DMAEMA-co-SMA)-1-Curcumine (blue line).*

FTIR spectroscopy was utilized in order to gain more information on the structure and interactions of the chimeric nnosystems. The comparison of ATR-FTIR spectra of random copolymers, DMPC and curcumin-loaded DMPC:P(DMAEMA-*co*-SMA) samples is shown in Fig. 40, in which the characteristic peaks are presented. The OH in 3450 cm^{-1} and the C=O in 1624 cm^{-1} and 1580 cm^{-1} prove the existence of curcumin in the hybrid samples,[82] while 1232 cm^{-1} and 1085 cm^{-1} peaks coming from the PO_2 group depict the existence of DMPC phospholipids.[83] The C=O in 1710 cm^{-1} is common for both the random copolymers samples

and DMPC phospholipids, while the C-O-C in 1100 cm^{-1} and the C-N in 970 cm^{-1} prove the existence of the PDMAEMA-co-PSMA copolymers.

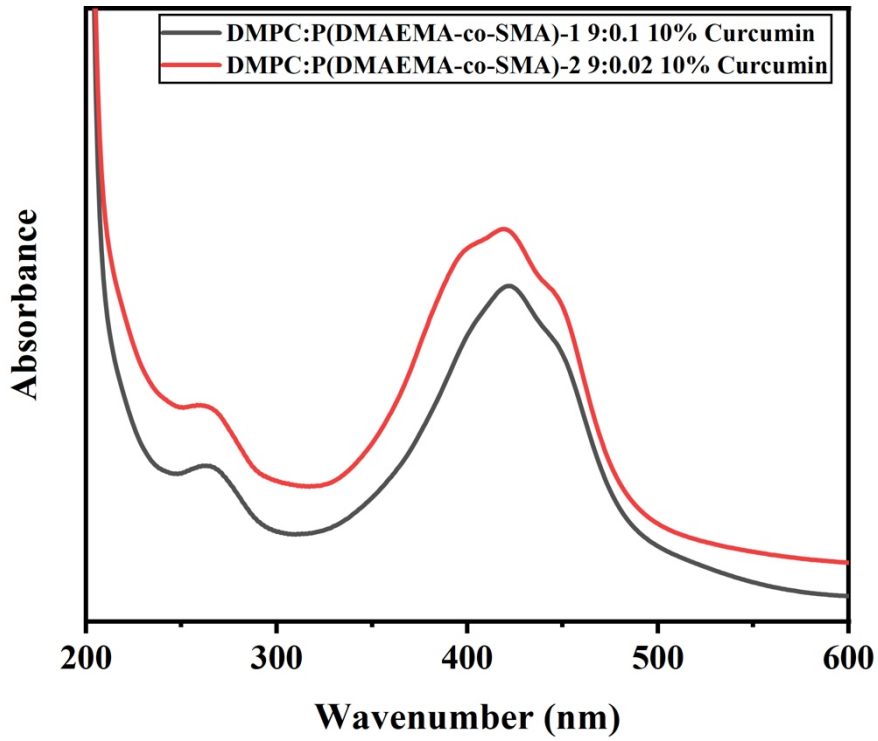

***Figure 41** : UV-Vis spectrum of DMPC:P(DMAEMA-co-SMA) samples loaded with 10% w/w curcumin*

UV-Vis spectrum for 10% w/w curcumin-loaded DMPC:P(DMAEMA-*co*-SMA) samples depicts the existence of curcumin with two characteristic absorbance peaks at 450 and 250 nm, respectively, according to literature data.

DISCUSSION

PDMAEMA is a hydrophilic, cationic, pH and thermo-responsive polymer, with a pK_a = 6.5 and a lower critical solution temperature ranging from 35^{o}C to 45^{o}C , depending mostly on the polymer's molecular weight. PSMA, on the other side, is a strongly hydrophobic polymer with a long hydrocarbon side chain.

The synthesis of P(DMAEMA-*co*-SMA) was accomplished by free-radical polymerization, a synthesis technique known to easily produce random copolymers with low cost, but also having a rather low polymerization control. Thus, two broadly polydisperse P(DMAEMA-*co*-SMA) random copolymers were synthesized, composed of 20% and 40% hydrophobic PSMA, as calculated from NMR spectra. Both FTIR and NMR spectra depict the existence of characteristic groups for both polymers, proving the successful synthesis.

Dynamic light scattering studies for the random copolymers, conducted in pH 3 and pH 7 aqueous solutions, and within a temperature range of 25^{o}C - 55^{o}C, showed a pH and thermo-responsive behavior coming from the DMAEMA segments. More specifically, when in pH 3 aqueous solution, the system presents improved solubility and no thermo-responsiveness, due to the fact that DMAEMA segments are fully protonated, while in pH 7 aqueous solution the system presents thermo-responsiveness coming from the partially-protonated DMAEMA segments.

CONTIN analysis of the DLS correlation functions of the two random copolymers show the existence of two large-polydispersed size-populations, one associated with unimers and the other with large aggregates. These size-populations are affected by temperature rise above PDMAEMA's LCST, forming large aggregates in the case of P(DMAEMA-*co*-SMA)-1 and small but large polydispersed nanoparticles in the case of P(DMAEMA-*co*-SMA)-2.

Micropolarity environment studies for both random copolymers show the existence of extremely hydrophobic domains, while ζ-potential depicts a huge difference in cationic surface charge between pH 3 and pH 7 solutions, due to the protonation ability of the DMAEMA component.

The preparation of the chimeric/hybrid liposomes with functional polymers was accomplished by thin-film hydration protocol, with a concentration of 10 mg / 1 ml, followed by 5-minute tip-sonication. The two random copolymer samples were mixed with 1,2-dimyristoyl-sn-glycero-3-phosphocholine (DMPC) (Fig.), a phospholipid with T_m = 22°C at 9:0.02 and 9:01 molar ratios. The reason lies to the fact that both random copolymers have high molecular weight values and could disrupt the viability of the phospholipid bilayers.

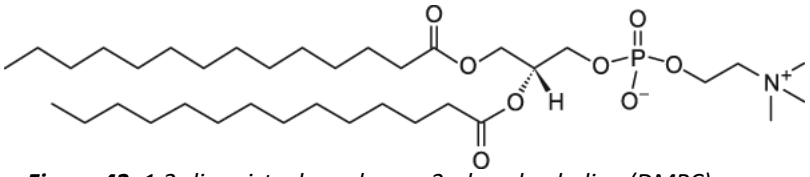

***Figure 42**: 1,2-dimyristoyl-sn-glycero-3-phosphocholine (DMPC)*

The four prepared phospholipid/copolymer formulations were characterized with dynamic and electrophoretic light scattering and photoluminescence spectroscopy, as aqueous solutions of pH 3 and pH 7 in a temperature range of 25°C - 55°C, in order to investigate their functionality.

DLS studies in pH 7 aqueous solutions for all DMPC:P(DMAEMA-*co*-SMA) samples show the formation of one well-defined size population, with R_h values ranging from 9 to 300 nm. The composition of hydrophilic/hydrophobic components and the molar ratio play a key role for both the self-assembly of the formed nanoparticles and their stability. More specifically, DMPC:-P(DMAEMA-*co*-SMA)-1 9:0.02 sample was unstable upon dilution, probably because the amount of hydrophobic content is under the lowest threshold value for the specific system. Raising the w/w ratio to 9:01 for the DMPC:P(DMAEMA-*co*-SMA)-1 led to stable nanoassemblies with R_h of 9 nm, stable enough for 2 months after their preparation. For the DMPC:P(DMAEMA-*co*-SMA)-2 samples, the random copolymers were composed of 40% hydrophobic segments, enough to provide the required stability even for the 9:0.02 molar ratio sample, while raising further the molar ratio to 9:0.1 resulted in larger nanoparticles.

In all cases, the resulted nanoassemblies exhibited thermo-responsive behavior, coming from the DMAEMA segments, which are partially protonated at pH 7. Differences in lipid/copolymers molar ratio, and even the copolymers composition, resulted in unique thermo-responsive behavior for each chimeric sample, as depicted in Table 6. The DMPC:-P(DMAEMA-*co*-SMA)-1 9:0.02 sample created large aggregates with a sudden R_h transition,

while the 9:0.1 samples created large aggregates with a linear R_h increase. On the other hand, the DMPC:P(DMAEMA-*co*-SMA)-2 samples presented a sudden decrease in their nanoparticles size with a sudden transition in R_h values, followed by a sharp increase of their mass, depicting a loss in internally bound water.

***Table 6**: R_h values for 25°C/55°C in pH 7 aqueous solutions*

Sample	R_h (nm) in 25°C	R_h (nm) in 55°C
P(DMAEMA-*co*-SMA)-1	9 and 35	900-
P(DMAEMA-*co*-SMA)-2	9 and 120	19
DMPC:P(DMAEMA-*co*-SMA)-1	19	900
DMPC:P(DMAEMA-*co*-SMA)-1	9	11, 90, 800
DMPC:P(DMAEMA-*co*-SMA)-2	300	220
DMPC:P(DMAEMA-*co*-SMA)-2	82	52

DLS studies for pH 3 aqueous solutions of all DMPC:P(DMAEMA-*co*-SMA) samples show the existence of one broad size-population (Fig), or even two well-defined populations in the case of DMPC:P(DMAEMA-*co*-SMA)-1 9:0.1(Fig). In pH 3 aqueous solution, the PDMAEMA segments become fully protonated and thus extremely hydrophilic, and do not exhibit thermo-responsive behavior.

Micro polarity studies on all samples depict the existence of hydrophobic domains in all chimeric nanosystemss. I_1/I_3 values get lower as the hydrophobic composition increases. Z-potential studies depict the cationic charge of the chimeric nanoparticles, which increases in pH 3 aqueous solutions, depicting the protonation of the DMAEMA segments.

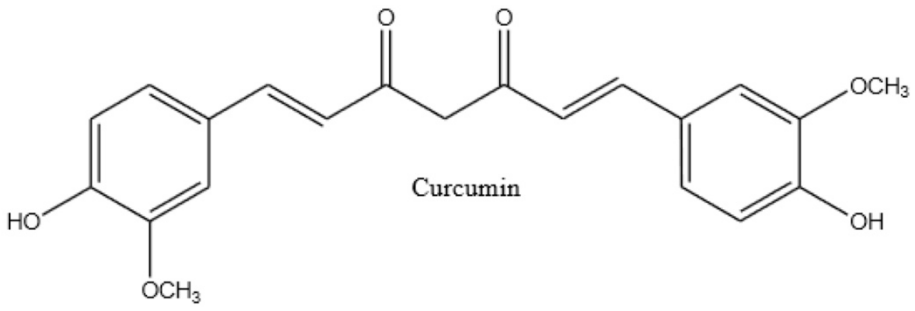

***Figure 43**: Chemical structure of curcumin*

The DMPC:P(DMAEMA-*co*-SMA)-1 9:0.1 and DMPC:P(DMAEMA-*co*-SMA)-2 9:0.02 chimeric samples were chosen for further loading with 10% and 20% w/w curcumin, due to their extreme stability and their preferable nanoassemblies size. Curcumin is a hydrophobic molecule that is claimed to present anti-inflammatory, anti-oxidant and anti-cancer properties.[84]. The drug-loading preparation was carried out by thin-film hydration, followed by double 5-minute tip-sonication. Both the 20% w/w curcumin-loaded DMPC:P(DMAEMA-*co*-SMA) samples were precipitated within 24 hours.

DLS studies on the 10% w/w curcumin-loaded DMPC:P(DMAEMA-*co*-SMA)-1 9:0.1 and DMPC:P(DMAEMA-*co*-SMA)-2 9:0.02 samples on pH 7 showed the existence of one well-defined size-population, with R_h at 200 and 300 nm respectively. Both samples exhibited a thermo-responsive behavior when heated after 35^{o}C, same as their non-curcumin loaded analogs. More specifically, for the first chimeric nanosystem, temperature rise to 55^{o}C leads to higher values of R_h, at 650 nm, with a broadened size-distribution, while the second chimeric nanosystem seems to disassociate into two smaller and well-defined size populations at 90 and 30 nm respectively.

Lowering the aqueous solutions pH to 3 for both curcumin-loaded chimeric samples leads to the formation of two co-existing size-populations at around 100 and 1000 nm respectively, while temperature rise to 55^{o}C leads to the broadening and merging of both size-populations.

UV-Vis spectrum analysis for both chimeric samples proves the existence of curcumin within the aqueous solutions, by depicting the characteristic absorbance peaks for the specific molecule at 250 and 450 nm respectively.

CONCLUSIONS

In the present study, two Poly((dimethyl amino ethyl methacrylate)-*co*-(stearyl methacrylate)) (P(DMAEMA-*co*-SMA)) random copolymers were successfully synthesized via free-radical polymerization, resulting in different compositions of 20% and 40%wt in hydrophobic PSMA content. DLS studies on aqueous solutions for both random copolymers showed a thermo and pH-responsive behavior. More specifically, pH 7 aqueous solutions studies showed that the random copolymers present thermo-responsive behavior when temperature exceeds the 35^{o}C threshold. Also, lowering the pH of the aqueous solution to 3 results in alteration of the nanoparticulate formations observed at pH 7, leading to broader size-distributions and loss of thermo-responsiveness, due the full protonation of the DMAEMA segments.

During the next step of the study, the successful preparation of chimeric/hybrid structures occurred by employing 1,2-dimyristoyl-sn-glycero-3-phosphocholine (DMPC) and the two previously synthesized random copolymers in a molar ratio of 9:0.1 and 9:0.02. Thus, four (4) DMPC:P(DMAEMA-*co*-SMA) samples were prepared through thin-film hydration protocol, followed by a double 5-minute tip-sonication. All chimeric/hybrid samples exhibited pH and thermo-responsiveness, as shown by DLS studies, while presented considerable cationic surface charge and extremely hydrophobic domains. The DMPC:P(DMAEMA-*co*-SMA)-1 9:0.1 and the DMPC:P(DMAEMA-*co*-SMA)-2 9:0.02 presented the most favorable structural characteristics and colloidal stability and thus were chosen for drug-loading with curcumin and further aqueous solution studies. All DMPC:P(DMAEMA-*co*-SMA) samples presented extreme stability, except DMPC:P(DMAEMA-*co*-SMA)-1 9:0.02, due to the low random copolymer hydrophobic content.

Four DMPC:P(DMAEMA-*co*-SMA) with 10% and 20% w/w curcumin-loaded samples were prepared with the same protocol utilized for the chimeric/hybrid samples. The 20% w/w curcumin-loaded samples were precipitated in a 24-hour time period. DLS studies of the 10% w/w curcumin-loaded samples showed the formation of rather large, but well-defined size-populations at 200 and 300 nm respectively. Both samples presented pH and thermo-responsiveness in such way that probably ruptures the lipid bilayer, resulting in the release of the loaded curcumin. It is extremely important to mention that DMPC:P(DMAEMA-*co*-SMA)-2 9:0.02 10% w/w curcumin-loaded sample was precipitated a week after its preparation, while

the DMPC:P(DMAEMA-*co*-SMA)-1 9:0.1 10% w/w curcumin-loaded sample is still stable after 3-months-time period.

Summing up, the resulting DMPC:P(DMAEMA-*co*-SMA) chimeric/hybrid structures can be potential nanocarriers for drug delivery, presenting preferable properties regarding loading of hydrophobic molecules under certain pH and temperature conditions.

REFERENCES

1. Suarez-Martinez, I.; Grobert, N.; Ewels, C. P., Encyclopedia of Carbon Nanoforms. In *Advances in Carbon Nanomaterials: Science and Applications*, Tagmatarchis, N., Ed. 2012; pp 1-52.
2. Low, J.; Yu, J.; Ho, W., Graphene-Based Photocatalysts for CO2 Reduction to Solar Fuel. *J Phys Chem Lett* **2015,** *6* (21), 4244-51.
3. Curtis, A.; Wilkinson, C., Nantotechniques and approaches in biotechnology. *Trends Biotechnol* **2001,** *19* (3), 97-101.
4. Demetzos, C., Introduction to Nanotechnology. In *Pharmaceutical Nanotechnology: Fundamentals and Practical Applications*, C., D., Ed. 2016; pp 3-16.
5. Kargozar, S.; Mozafari, M., Nanotechnology and Nanomedicine: Start small, think big. *Materials Today: Proceedings* **2018,** *5*, 15492-15500.
6. Leonhardt, U., Invisibility Cup. *Nature Photonics* **2007,** *1*, 207-208.
7. Verhoeven, J., The Mystery of the Damascus Sword. *Muse* **1998,** *2* (2), 35-43.
8. Benelmekki, M., An Introduction to Nanoparticles and Nanotechnology. In *Designing Hybrid Nanoparticles*, 2015; pp 1-14.
9. Behari, J., Principles of nanoscience: an overview. *Indian J Exp Biol* **2010,** *48* (10), 1008-19.
10. Logothetidis, S., Nanotechnology: Principles and Applications. In *Nanostructured Materials and Their Applications. NanoScience and Technology*, Logothetidis, S., Ed. Springer: Heidelberg, Berlin, 2012.
11. https://en.wikipedia.org/wiki/Richard_Feynman.
12. https://alchetron.com/Norio-Taniguchi.
13. https://en.wikipedia.org/wiki/K._Eric_Drexler.
14. Duriagina, Z.; Holyaka, R.; Tepla, T.; Kulyk, V.; Arras, P.; Eyngorn, E., Identification of Fe3O4 Nanoparticles Biomedical Purpose by Magnetometric Methods. In *Biomaterials in Regenerative Medicine*, 2018; pp 379-407.
15. Soares, S.; Sousa, J.; Pais, A.; Vitorino, C., Nanomedicine: Principles, Properties, and Regulatory Issues. *Frontiers in Chemistry* **2016,** *6*, 350.
16. Rakhimol, K. R.; Augustine, R.; Thomas, S.; Kalarikkal, N., Nanomedicine: From Concept to Reality. In *Nanomedicine and Tissue Engineering: State of the Art and Recent Trends*, 2016; pp 1-31.
17. Demetzos, C., Applications of Nanotechnology in Drug Delivery and Targeting. In *Pharmaceutical Nanotechnology: Fundamentals and Practical Applications*, Demetzos, C., Ed. 2016; pp 77-142.
18. Dhoke, D. M.; Chikhale, R. V.; Pant, A. M.; Menghani, S.; N, N. R.; Khedekar, P. B., Recent Advances in Nanoparticulate Drug Delivery System for Antiviral Drugs. In *Nanomedicine and Tissue Engineering: State of the Art and Recent Trends*, 2016; pp 183-218.
19. Demetzos, C.; Pippa, N., Advanced drug delivery nanosystems (aDDnSs): a mini-review. *Drug Deliv* **2014,** *21* (4), 250-7.
20. Makhlouf, A. S. H.; Abu-Thabit, N. Y., *Stimuli Responsive Polymeric Nanocarriers for Drug Delivery Applications: Types and Triggers*. 2018; Vol. 1.
21. Naziris, N.; Pippa, N.; Pispas, S.; Demetzos, C., Stimuli-responsive Drug Delivery Nanosystems: From Bench to Clinic. *Current Nanomedicine* **2016,** *6*, 1-20.

22. Demetzos, C., Applications of Nanotechnology in Imaging and Diagnostics. In *Pharmaceutical Nanotechnology: Fundamentals and Practical Applications*, 2016; pp 65-76.
23. Power, S.; Slattery, M. M.; Lee, M. J., Nanotechnology and its relationship to interventional radiology. Part I: imaging. *Cardiovasc Intervent Radiol* **2011,** *34* (2), 221-6.
24. Nie, L.; Wang, S.; Wang, X.; Rong, P.; Ma, Y.; Liu, G.; Huang, P.; Lu, G.; Chen, X., In vivo volumetric photoacoustic molecular angiography and therapeutic monitoring with targeted plasmonic nanostars. *Small* **2014,** *10* (8), 1585-93, 1441.
25. Draz, M. S.; Kochehbyoki, K. M.; Vasan, A.; Battalapalli, D.; Sreeram, A.; Kanakasabapathy, M. K.; Kallakuri, S.; Tsibris, A.; Kuritzkes, D. R.; Shafiee, H., DNA engineered micromotors powered by metal nanoparticles for motion based cellphone diagnostics. *Nat Commun* **2018,** *9* (1), 4282.
26. Khadem-Abbassi, K.; Rinnert, H.; Balan, L.; Doumandji, Z.; Joubert, O.; Masteri-Farahani, M.; Schneider, R., CdTe0.5S0.5/ZnS Quantum Dots Embedded in a Molecularly Imprinted Polymer for the Selective Optosensing of Dopamine. *Nanomaterials (Basel)* **2019,** *9* (5), 693.
27. Cui, Y.; Wei, Q.; Park, H.; Lieber, C. M., Nanowire nanosensors for highly sensitive and selective detection of biological and chemical species. *Science* **2001,** *293* (5533), 1289-92.
28. Wang, Y.; Wanzhi, W.; Xiaoying, L.; Xiandong, Z., Carbon nanotube/chitosan/ gold nanoparticles-based glucose biosensor prepared by a layer-by-layer technique. *Mater Sci Eng* **2009,** *29* (1), 50-54.
29. Liu, G.; Mao, X.; Phillips, J. A.; Xu, H.; Tan, W.; Zeng, L., Aptamer-nanoparticle strip biosensor for sensitive detection of cancer cells. *Anal Chem* **2009,** *81* (24), 10013-8.
30. Kalarikkal, N.; Augustine, R.; Oluwafemi, O. S.; Joshy, K. S.; Thomas, S., *Nanomedicine and Tissue Engineering: State of the Art and Recent Trends*. 2016.
31. Smith, W. R.; Hudson, P. W.; Ponce, B. A.; Rajaram Manoharan, S. R., Nanotechnology in orthopedics: a clinically oriented review. *BMC Musculoskelet Disord* **2018,** *19* (1), 67.
32. Garimella, R.; Eltorai, A. E., Nanotechnology in orthopedics. *J Orthop* **2017,** *14* (1), 30-33.
33. Mazaheri, M.; Eslahi, N.; Ordikhani, F.; Tamjid, E.; Simchi, A., Nanomedicine applications in orthopedic medicine: state of the art. *Int J Nanomedicine* **2015,** *10*, 6039-53.
34. Gheibi Hayat, S. M.; Darroudi, M., Nanovaccine: A novel approach in immunization. *J Cell Physiol* **2019,** *234* (8), 12530-12536.
35. K.S.Yadav, H.; Dibi, M.; Mohammad, A.; Srouji, A. E., Nanovaccines formulation and applications-a review. *Journal of Drug Delivery Science and Technology* **2018,** *44*, 380-387.
36. Sekhon, B. S.; Saluja, V., Nanovaccines-An overview. *IJPFR* **2011,** *1* (1), 101-109.
37. Mortimer, G. M.; Minchin, R. F., Nanotoxicology and Nanovaccines. In *Micro and Nanotechnology in Vaccine Development: Micro and Nano Technologies*, 2017; pp 373-392.
38. Dobrovolskaia, M. A.; Shurin, M.; Shvedova, A. A., Current understanding of interactions between nanoparticles and the immune system. *Toxicology and applied pharmacology* **2016,** *299*, 78-89.
39. Haase, A.; Dommershausen, N.; Schulz, M.; Landsiedel, R.; Reichardt, P.; Krause, B. C.; Tentschert, J.; Luch, A., Genotoxicity testing of different surface-functionalized SiO2, ZrO2 and silver nanomaterials in 3D human bronchial models. *Arch Toxicol* **2017,** *91* (12), 3991-4007.
40. Demetzos, C., Nanotoxicity and Biotoxicity. In *Pharmaceutical Nanotechnology: Fundamentals and Practical Applications*, Demetzos, C., Ed. Springer Nature: 2016; pp 175-188.

41. Jain, K. K., Future of nanomedicine: impact on healthcare & society. *Nanomedicine (Lond)* **2015,** *10* (21), 3199-202.
42. Jain, K. K., *Textbook of Personalized Medicine*. Springer: 2015.
43. Ebewele, R. O., *Polymer Science and Technology*. CRC Press: New York, 2000.
44. Cowie, J. M. G.; Arrighi, V., *Polymers: Chemistry and Physics of Modern Materials*. 2007.
45. Odian, G., *Principles of Polymerization*. 2004.
46. Moad, G.; Solomon, D. H., *The Chemistry of Radical Polymerization*. Elsevier: 2006.
47. Callister, W. D., *Fundamentals of Materials Science and Engineering*. 2001.
48. Wei, M. L.; Gao, Y. F.; Li, X.; Serpe, M. J., Stimuli-responsive polymers and their applications. *Polymer Chemistry* **2017,** *8* (1), 127-143.
49. Cabane, E.; Zhang, X.; Langowska, K.; Palivan, C. G.; Meier, W., Stimuli-responsive polymers and their applications in nanomedicine. *Biointerphases* **2012,** *7* (1-4), 9.
50. Bawa, P.; Pillay, V.; Choonara, Y. E.; du Toit, L. C., Stimuli-responsive polymers and their applications in drug delivery. *Biomed Mater* **2009,** *4* (2), 022001.
51. Gao, X.; Cao, Y.; Song, X.; Zhang, Z.; Xiao, C.; He, C.; Chen, X., pH- and thermo-responsive poly(N-isopropylacrylamide-co-acrylic acid derivative) copolymers and hydrogels with LCST dependent on pH and alkyl side groups. *Journal of Materials Chemistry B* **2013,** *1* (41).
52. Fujii, S.; Mouri, E.; Akiyama, K.; Nakayama, S.; Uda, K.; Nakamura, Y.; Matsuoka, H., pH-Sensitive Adsorption Behavior of Polymer Particles at the Air-Water Interface. *Langmuir* **2017,** *33* (6), 1451-1459.
53. Niskanen, J.; Wu, C.; Ostrowski, M.; Fuller, G. G.; Hietala, S.; Tenhu, H., Thermoresponsiveness of PDMAEMA. Electrostatic and Stereochemical Effects. *Macromolecules* **2013,** *46* (6), 2331-2340.
54. Ahmed, M. R.; Mohammed, A. H. A. K.; A.hamad, M., Synthesis, Characterization and Performance Evaluation of Poly Octadecyl Methacrylate and Poly Octadecyl Methacrylate-CoMethylmethacrylate as an Additive for Lubricating Oil. *IOSR Journal of Applied Chemistry* **2017,** *10* (04), 50-58.
55. Gombotz, W. R., Liposomes. In *Biomaterials Science*, 2013; pp 1039-1041.
56. Bangham, A. D.; Horne, R. W.; Glauert, A. M.; Dingle, J. T.; Lucy, J. A., Action of saponin on biological cell membranes. *Nature* **1962,** *196*, 952-5.
57. Horne, R. W.; Bangham, A. D.; Whittaker, V. P., Negatively Stained Lipoprotein Membranes. *Nature* **1963,** *200*, 1340.
58. Weissmann, G.; Sessa, G.; Standish, M.; Bangham, A. D., Abstracts. *Journal of Clinical Investigation* **1965,** *44* (6), 1072-1116.
59. Watts, G., Alec Douglas Bangham. *The Lancet* **2010,** *375* (9731).
60. Akbarzadeh, A.; Rezaei-Sadabady, R.; Davaran, S.; Joo, S. W.; Zarghami, N.; Hanifehpour, Y.; Samiei, M.; Kouhi, M.; Nejati-Koshki, K., Liposome: classification, preparation, and applications. *Nanoscale Res Lett* **2013,** *8* (1), 102.
61. Allen, T. M.; Cullis, P. R., Liposomal drug delivery systems: from concept to clinical applications. *Adv Drug Deliv Rev* **2013,** *65* (1), 36-48.
62. B., F. D.; R., C. P., Encapsulation of Weakly-Basis Drugs, Antisense Oligonucleotides and Plasmid DNA within Large Unilamellar Vesicles for Drug Delivery Applications. In *Liposomes, a Practical Approach*, Oxford University: 2003; pp 173-180.
63. Jiang, W.; Lionberger, R.; Yu, L. X., In vitro and in vivo characterizations of PEGylated liposomal doxorubicin. *Bioanalysis* **2011,** *3* (3), 333-44.

64. Balasegaram, M.; Ritmeijer, K.; Lima, M. A.; Burza, S.; Genovese, G. O.; Milani, B.; Gaspan, S.; Potet, J.; Chappuis, F., Liposomal Amphotericin B as a Treatment for Human Leishmaniasis. *Expert Opin. Emerg. Drugs* **2012,** *17*, 493-510.
65. Sercombe, L.; Veerati, T.; Moheimani, F.; Wu, S. Y.; Sood, A. K.; Hua, S., Advances and Challenges of Liposome Assisted Drug Delivery. *Front Pharmacol* **2015,** *6*, 286.
66. Gabizon, A. A.; Shmeeda, H.; Zalipsky, S., Pros and cons of the liposome platform in cancer drug targeting. *J Liposome Res* **2006,** *16* (3), 175-83.
67. Naziris, N.; Pippa, N.; Meristoudi, A.; Pispas, S.; Demetzos, C., Design and development of pH-responsive HSPC:C12H25-PAA chimeric liposomes. *J Liposome Res* **2017,** *27* (2), 108-117.
68. Naziris, N.; Pippa, N.; Stellas, D.; Chrysostomou, V.; Pispas, S.; Demetzos, C.; Libera, M.; Trzebicka, B., Development and Evaluation of Stimuli-Responsive Chimerinc Nanostructures. *AAPS PharmSciTech* **2018,** *18* (7), 2971-2989.
69. Yamazaki, N.; Sugimoto, T.; Fukushima, M.; Teranishi, R.; Kotaka, A.; Shinde, C.; Kumei, T.; Sumida, Y.; Munekata, Y.; Maruyama, K.; Yba, E.; Harada, A.; Kono, K., Dual-Stimuli Responsive Liposomes using pH- and Temperature Sensitive Polymers for Controlled Transdermal Delivery. *Polym. Chemi.* **2017,** *8*, 1507-1518.
70. Naziris, N.; Pippa, N.; Stellas, D.; Chrysostomou, V.; Pispas, S.; Demetzos, C.; Libera, M.; Trzebicka, B., Morphological Diversity of Block Copolymer/Lipid Chimeric Nanostructures. *J. Nanopart Res.* **2017,** *19*, 347.
71. Pippa, N.; Kaditi, E.; Pispas, S.; Demetzos, C., PEO-b-PCL:DPPC Chimeric Nanocarriers: Self-Assembly Aspects in Aqueous and Biological Media and Drug Incorporation. *Soft Matter* **2013,** *9*, 4073-4082.
72. Lee, S. M.; Nguyen, S. T., Smart Nanoscale Drug Delivery Platforms from Stimuli-Responsive Polymers and Liposomes. *Macromolecules* **2013,** *46* (23), 9169-9180.
73. Smith, B. C., The Basics of Infrared Interpretation. In *Infrared Spectral Interpretation: A Systematic Approach*, pp 1-30.
74. Socrates, G., Introduction. In *Infrared and Raman Characteristic Group Frequencies*, Socrates, G., Ed. John Willey and Sons: pp 1-48.
75. Macomber, R. S., *A Complete Introduction to Modern NMR Spectroscopy*. John Wiley and Sons: 1998.
76. Carbajo, R. J.; Neira, L., The Basis of Nuclear Magnetic Resonance Spectroscopy. In *NMR for Chemists and Biologists*, Springer: 2013.
77. Trathnigg, B., Size-exclusion Chromatography of Polymers. In *Encyclopedia of Analytical Chemistry*
, Meyers, R. A., Ed. John Wiley & Sons Ltd: Chichester, 2000; pp 8008–8034.
78. Schartl, W., *Light Scattering from Polymer Solutions and Nanoparticle Dispersions*. Springer: 2007.
79. Xu, R., Electrophoretic Light Scattering: Zeta Potential Measurment. In *Particle Characterization: Light Scattering Methods*, Scarlett, B., Ed. Springer: 1998; pp 289-343.
80. Limpouchova, Z.; Prochazka, K., Theoretical Principles of Fluorescence Spectroscopy. In *Fluorescence Studies of Polymer Containing Systems*, Procházka, K., Ed. Springer: 2016.
81. Owen, T., *Fundamentals of UV-visible Spectroscopy: A Primer*. 1996.
82. Madhavi, M.; Madhavi, K.; Jithan, A. V., Preparation and in vitro/in vivo characterization of curcumin microspheres intended to treat colon cancer. *J Pharm Bioallied Sci* **2012,** *4* (2), 164-71.

83. Bridelli, M. G.; Capelletti, R.; Mora, C., Structural features and functional properties of water in model DMPC membranes: thermally stimulated depolarization currents (TSDCs) and Fourier transform infrared (FTIR) studies. *J. Phys. D: Appl. Phys* **2013,** *46*, 485401.
84. Rohman, A., Analysis of curcuminoids in food and pharmaceutical products. *Int Food Res J* **2012,** *19* (1), 19-27.